Mechanical Systems and Signal Processing 147 (2021) 107116

Contents lists available at ScienceDirect

Mechanical Systems and Signal Processing

journal homepage: www.elsevier.com/locate/ymssp

Factorized wave propagation model in tree-type pipe networks and its application to leak localization

Xun Wang [a,b,*], G. Adriana Camino [b], Tong-Chuan Che [b], Mohamed S. Ghidaoui [b]

[a] Key Laboratory on Reliability and Environmental Engineering Technology, School of Reliability and Systems Engineering, Beihang University, Xueyuan Road No. 37, Haidian District, Beijing 100083, China

[b] Department of Civil and Environmental Engineering, Hong Kong University of Science and Technology, Clear Water Bay, Hong Kong, China

ARTICLE INFO

Article history:
Received 6 December 2019
Received in revised form 12 June 2020
Accepted 30 June 2020

Keywords:
Pipe network
Tree network
Leak localization
Transient wave
Matched-field processing

ABSTRACT

In a leaky tree-structured pipe network, transient head and discharge at a measurement location arise from a superposition of the waves along the set of pipes linking the measurement location to each boundary node. Moreover, the solution can be split into a leak-free part and a term that accounts for the scattering from the leak, the latter varies linearly with leak size and nonlinearly with leak location. It is then shown that if the head adjacent to each boundary node is measured, any reasonably-sized leak can be uniquely and efficiently identified by the matched-field processing approach. The efficiency of the leak identification scheme stems from the linear dependence of wave scattering on leak size. The proposed method is successfully applied both numerically and to pilot data from a tree-structured system of viscoelastic pipes.

1. Introduction

Leak localization in water supply systems is an important problem since leakage results in a huge wastage of water resources, as well as health risks because leaks are potential entry points for contaminants. Transient wave-based leakage detection methodology has been intensively investigated since the 1990s [1–6]. The idea of this methodology is to introduce active pressure waves in pipe systems by sudden operation of valves or other devices. The waves propagate back and forth in the pipe system, interact with leaks, and thus carry information about the features of leaks in the pipe. By measuring and analyzing the pressure response, leaks in water pipe systems can be estimated. Specific transient-based leakage detection approaches can be classified as: (i) transient reflection-based method (TRM) [5,7–11]; (ii) frequency response feature method (FRFM) [4,12–18]; (iii) time-domain full-wave inversion (FWI) method [2,3,19–22]; and (iv) frequency-domain FWI method [6,15,23–27].

While most of the transient-based methods consider single and relatively simple pipeline systems, some researches have generalized these methods to pipe networks. The wavelet transform analysis (WTA) [10,28], the cross-correlation analysis [29], the impulse response function method [11], and the instantaneous frequency analysis techniques [30], as representatives of TRM, have been applied to detect leaks in pipe networks. These methods extract the arrival time of reflection from a leak, which can decide the distance from the leak to the sensor, but cannot know the exact location

* Corresponding author at: Key Laboratory on Reliability and Environmental Engineering Technology, School of Reliability and Systems Engineering, Beihang University, Xueyuan Road No. 37, Haidian District, Beijing 100083, China.
E-mail address: xunwang@buaa.edu.cn (X. Wang).

https://doi.org/10.1016/j.ymssp.2020.107116
0888-3270/

Nomenclature

q	discharge oscillation
h	head oscillation
$\mathcal{X}$	coordinate system of pipe network
$\partial\mathcal{X}$	boundaries of $\mathcal{X}$
$\mathcal{J}$	interior junctions of $\mathcal{X}$
$\mathcal{V}$	valve in $\mathcal{X}$
x^L	leak location
z^L	pipe elevation at leak
s^L	leak size
x^U (x^D)	upstream (downstream) boundary
Q_0^L, H_0^L	steady-state discharge and head of leak
Q_0	steady-state discharge of main pipe
x^M	sensor coordinate
$\Delta\mathbf{h}$	head difference
$\mathbf{n}$	measurement noise
a	wave speed
A	internal area of pipe
l	pipe length
d	internal diameter of pipe
e	pipe wall thickness
ω	angular frequency
FRF	frequency response function
FRFM	frequency response feature method
FWI	full-wave inversion
ITA	inverse transient analysis
MFP	matched-field processing
MOC	method of characteristics
RFPP	resonant frequency peak pattern
TRM	transient reflection-based method
SNR	signal-to-noise ratio
WTA	wavelet transform analysis

if the leak-sensor distance corresponds to more than one possible location in a complex network. Moreover, as these methods do not make full use of the measurement information (but only the leak reflection), they are not robust to noise and uncertainties and are thus limited in real applications. The resonant frequency peak pattern (RFPP) method (a representative of FRFM) [31] uses the damping of pressure amplitude at various resonant frequencies to estimate the leak. However, the pattern of the resonant frequency peaks is largely modified by other types of damping such as pipe viscoelasticity [25,32], hence this method has only limited applications. Again, since only a small portion (the resonant frequencies) of signal (in the frequency domain) is used, the RFPP method is also not robust to noise. The inverse transient analysis (ITA) method [2,3,33], as a representative of time-domain FWI, estimate the leak parameters by matching the time-domain transient wave model with the measured data. The FWI method is more robust than TRM and FRFM because more measurement information is used. However, since the time-domain model can only be solved numerically and the ITA method assumes a large number of unknown parameters, a high-dimensional optimization needs to be solved which is initialization-dependent and usually has the problem of local optimum traps [25]. As a matter of fact, in the considered pipe networks in [2,3,33], leaks can only be located at the junctions of pipes; assuming more potential leaks elsewhere in the pipe network would further increase the dimension of the optimization problem in the ITA methods. The computational complexity problem of ITA is partially solved by [34,35], which use the frequency-domain model where an analytical solution of wave propagation is available [36,37]. In [34,35], a leak in a Y-shape branched system is localized by a frequency-domain model-data matching. However, the methods in [34,35] still need to solve high-dimensional optimization problems, which therefore have the problems of local maximum traps and high computational costs, and neglect the influence of noise in solving the FWI.

This paper considers a frequency-domain wave propagation model in a general tree-structured pipe network. The classical frequency-domain transfer matrix model [38,39] is applied to the tree-structured network. The model is further explored such that the leak parameters to be estimated (leak location and size) are factorized. More exactly, the solution is split into a leak-free term and a term that represents the scattering from the leak which varies linearly with leak size and non-linearly with leak location. Based on this novel model which is more suitablefor leak parameter estimation, the leak localization in a pipe network is realized based on the matched-field processing (MFP) principle, which has been applied in

the leakage detection in single pipes [6,25]. Combining the parameter-factorized model and the MFP method, a fast 1D search of leak location (independent of leak size) in a pipe network is realized. The proposed method is able to localize a leak anywhere in a network and does not need any optimization technique. Furthermore, the MFP principle and sufficient use of measurement guarantee the robustness of the proposed method in noisy environments [25].

2. Factorized transient wave model in tree-structured pipe networks

An analytical solution of wave propagation in tree-structured pipe networks is next obtained, where the leak parameters (location and size) are factorized.

2.1. Topological structure

Wave propagation in tree-structured pipe networks [40] is studied. Networks with loop structures [41] are beyond the scope of the present paper. However, in real pipe systems where many isolating valves are often available, a loop network can be ideally converted into a tree network. A general tree network is denoted by $\mathcal{X}$ and is illustrated in Fig. 1(a). The nodes of the network include boundaries (denoted by $\partial\mathcal{X}$) and interior junctions (denoted by $\mathcal{J}$); all the other points ($x \in \mathcal{X} \setminus (\partial\mathcal{X} \cup \mathcal{J})$) in the system are called ordinary interior points. The boundaries $\partial\mathcal{X}$ of the network consist of all the nodes that are connected to only one pipe. At one (and only one) boundary, a valve, whose location is denoted by $\mathcal{V} \in \partial\mathcal{X}$, is set to generate transient waves. The interior junctions $\mathcal{J}$ are those nodes connected to at least two pipes. Note that an $x^j \in \mathcal{X}$ connecting to exactly two pipes is an interior junction (i.e., $x^j \in \mathcal{J}$) only if the two pipes have different properties (e.g., diameter, thickness, or material), which results in an impedance change and wave reflections at x^j; otherwise, it is just an ordinary interior point.

For the sake of clarity in describing the wave propagation paths, the nodes are divided into several levels. Level 0 has only one node where the wave-generating valve $\mathcal{V}$ is located. Level 1 has also only one node which connects the valve $\mathcal{V}$ by a single pipe. Each pipe in the network links two nodes in two adjacent levels. For each $x^j \in \mathcal{J}$, a unique mother pipe connects x^j to another node in x^j's lower level; all the other pipes connecting x^j to x^j's higher level nodes are called child pipes. Note that the aforementioned levels and mother/child pipes are introduced only to denote the tree network's structure; the (steady-state) flow direction in the pipe network is not necessarily from a high level to a low level or from mother to child pipes. Furthermore, if the location of wave-generating valve is switched to another $x \in \partial\mathcal{X}$, the levels of the nodes are also changed, as indicated in Fig. 1(b) as an example.

2.2. A general model

The discharge q and the head h[1] at the valve $\mathcal{V}$ are computed from all the other boundaries $\partial\mathcal{X} \setminus \mathcal{V}$. If q and h in $\partial\mathcal{X} \setminus \mathcal{V}$ are known (assumed, measured or computed), then q and h at any location in the network can be computed by the transfer matrix method. The detailed derivations of these boundary conditions (q and h in $\partial\mathcal{X} \setminus \mathcal{V}$) are presented in Section 2.4.

The number of pipes in the network is denoted by P and the numbering of the pipes is arbitrary. In the i-th pipe, $i \in \{1, \ldots, P\}$, the upstream node (which connects the i-th pipe to its child pipes) is x_i^U. Given $q(x_i^U)$ and $h(x_i^U)$, q and h at any x in this pipe are

$$\begin{pmatrix} q(x) \\ h(x) \end{pmatrix} = \mathbf{M}(x_i^U \to x) \begin{pmatrix} q(x_i^U) \\ h(x_i^U) \end{pmatrix}. \tag{1}$$

Here, $\mathbf{M}(x \to y)$ is the transfer matrix from the node x to y, where x and y are in the same single pipe. Eq. (1) is the linearized counterpart of the water-hammer equations in the frequency domain [38,39,45]. The explicit form of $\mathbf{M}(x \to y)$ depends on the existence of leak and is specified in Section 2.3.

For each interior junction $x^j \in \mathcal{J}$, the joint points in its mother pipe and in its child pipes are denoted by x^{jU} and $x_i^{jD}, i = 1, \ldots, n_j$ (n_j is the number of child pipes of x^j), respectively. More exactly, for example, x^{jU} is the limiting point of x which belongs to x^j's mother pipe and $x \to x^j$. By the pressure equilibrium and mass conservation conditions, q and h across x^j have the relationship of wave superposition [38,39]:

[1] Here, q and h are the frequency response functions (FRFs), i.e., the responses of discharge and head when an ideal impulse wave is sent in the system. In practice, any type of wave source (flow perturbation) is applicable and the FRFs can then be estimated using the methods in [7,11,24,42,43]. However, the flow perturbation has to be fast enough to excite transient waves with a sufficiently high bandwidth, which affects the accuracy and resolution of the leak localization [24]. In the experiments of the present paper (introduced in Section 5), the wave is generated by suddenly and fully closing a valve, i.e., a step wave is sent. If the strength of transient wave is too large, this operation may have the risk of pipe structural failure. Alternatively, the small-amplitude multi-test strategy [44] or sending a small-amplitude but long-time source-wave (such as the pseudo-random binary sequence) [7,11,43] can also successfully estimate the FRF, by which the risk can be reduced.

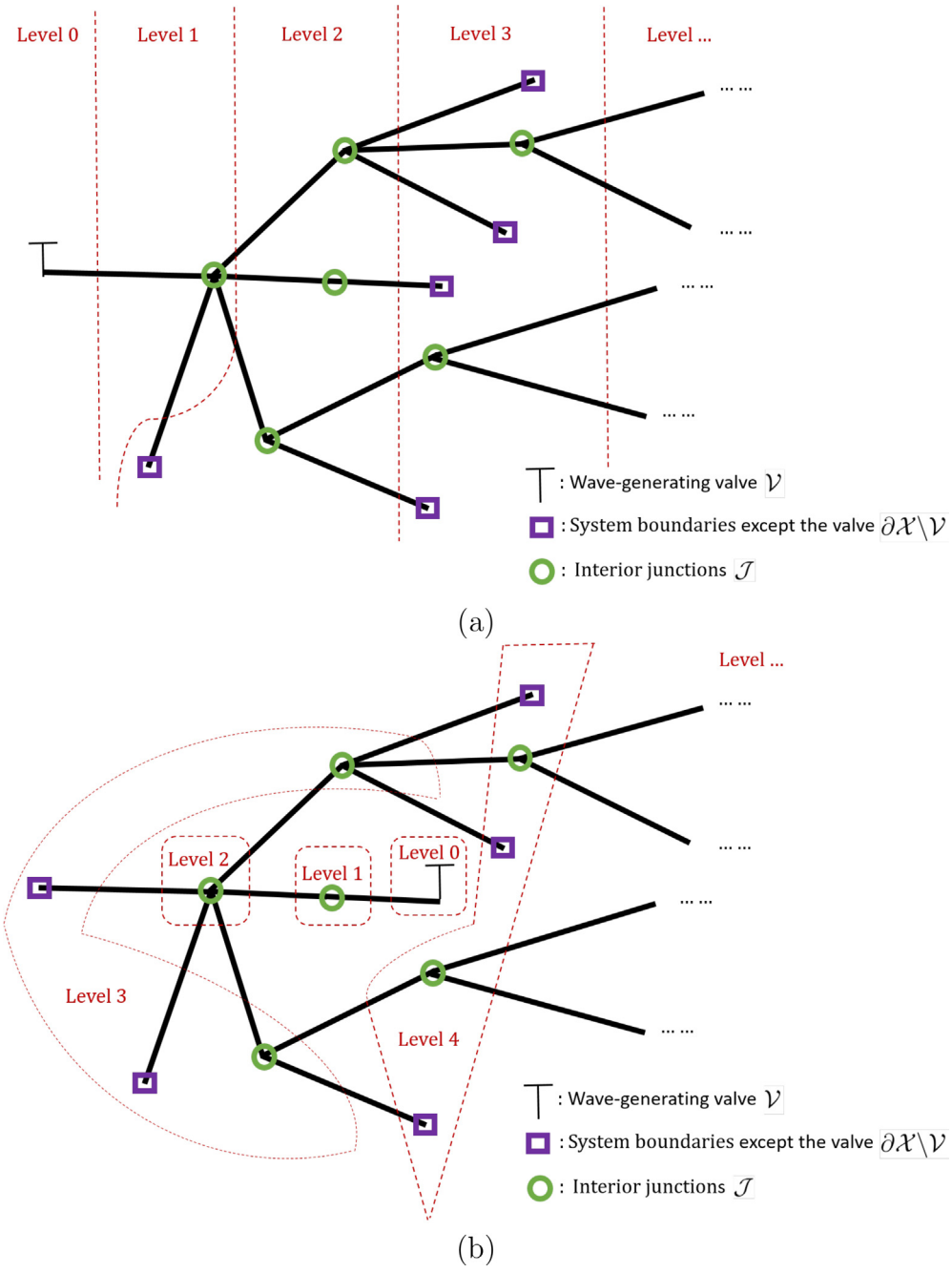

Fig. 1. (a) sketch of a tree-type pipe network; (b) the same network as (a) but the valve location is changed.

$$\begin{pmatrix} q\left(x^{JU}\right) \\ h\left(x^{JU}\right) \end{pmatrix} = \mathbf{I}_{22} \begin{pmatrix} q\left(x_1^{JD}\right) \\ h\left(x_1^{JD}\right) \end{pmatrix} + \sum_{i=1}^{n_J} (-1)^{\alpha_i} \mathbf{I}_{11} \begin{pmatrix} q\left(x_i^{JD}\right) \\ h\left(x_i^{JD}\right) \end{pmatrix}. \tag{2}$$

In this equation, $\mathbf{I}_{ij}$ is a 2-by-2 matrix where the element in i-th line and j-th column is 1 and all the other elements are 0. Besides, $\alpha_i = 0$ if x_i^{JD} has the same flow direction as x^{JU} and $\alpha_i = 1$ otherwise, which guarantees that the inflow and outflow across x^J are identical.

For the n-th boundary in $\partial\mathcal{X} \setminus \mathcal{V}$, denoted by $x_{n_1}^U \in \partial\mathcal{X} \setminus \mathcal{V}$, there exists a unique path from $x_{n_1}^U$ to $\mathcal{V}$, from the high level to the low level. If $x_{n_1}^U$ is in Level p_n, the path from $x_{n_1}^U$ to $\mathcal{V}$ includes p_n pipes and $p_n - 1$ interior junctions. Furthermore, for any

measurement point x^M in the network, the path from x^M towards its higher levels until some boundaries in $\partial\mathcal{X}\setminus\mathcal{V}$ is unique and used for simulating the wave propagation and measurement. For example, according to the wave propagation and superposition principles in Eqs. (1) and (2), the discharge and head at $x^M=\mathcal{V}$ are:

$$\begin{pmatrix} q(x^M) \\ h(x^M) \end{pmatrix} = \sum_{n=1}^{\mathrm{card}(\partial\mathcal{X}\setminus\mathcal{V})} \mathbf{M}\left(x^U_{n_{p_n}} \to x^M\right) \left(\prod_{i=p_n-1}^{1} \mathbf{I}^{(n_i)} \mathbf{M}\left(x^U_{n_i} \to x^D_{n_i}\right) \right) \begin{pmatrix} q\left(x^U_{n_1}\right) \\ h\left(x^U_{n_1}\right) \end{pmatrix}. \tag{3}$$

Here, we use the notation n_i ($n_i \in \{1,\dots,P\}$) to denote the index of the pipe, which is the i-th pipe in the path from the n-th boundary to $\mathcal{V}$. Furthermore, $x^U_{n_i}$ and $x^D_{n_i}$ are the upstream and downstream nodes of the pipe with index n_i, $\mathrm{card}(\partial\mathcal{X}\setminus\mathcal{V})$ is the cardinality of the set $\partial\mathcal{X}\setminus\mathcal{V}$, i.e., the number of boundaries except $\mathcal{V}$, $\mathbf{I}^{(n_i)} = \mathbf{I}_{22} + (-1)^{\alpha_{n_i}}\mathbf{I}_{11}$ if n_i is the first child pipe of its mother node and $\mathbf{I}^{(n_i)} = (-1)^{\alpha_{n_i}}\mathbf{I}_{11}$ otherwise. Note that since the wave propagation is computed from all the boundaries in $\partial\mathcal{X}\setminus\mathcal{V}$ to $\mathcal{V}$, Eq. (3) is a summation of $\mathrm{card}(\partial\mathcal{X}\setminus\mathcal{V})$ terms. Each term is a multiplication of $2p_n-1$ matrices if the path includes p_n pipes, in which the matrices $\mathbf{M}$ and $\mathbf{I}^{(n_i)}$ depict the wave propagations inside a pipe and across an interior junction, respectively. In the following, two examples of pipe network are presented where their explicit forms of Eq. (3) are given.

Example 1. The system is shown in Fig. 2 and is composed of three pipes. The i-th pipe ($i=1,2,3$) is bounded by the upstream node x^U_i and downstream node x^D_i. Actually, x^D_1, x^U_2, and x^D_3 are all located at the interior junction. However, they stand for locations in different pipes approximating to the junction. In this system, $\partial\mathcal{X}\setminus\mathcal{V} = \{x^U_1, x^U_3\}$ and $\mathcal{V} = \{x^D_2\}$, the two paths from the two boundaries $\partial\mathcal{X}\setminus\mathcal{V}$ to $\mathcal{V}$ are $x^U_1 \to x^D_1 \to x^U_2 \to x^D_2$ and $x^U_3 \to x^D_3 \to x^U_2 \to x^D_2$. However, the flow direction is different: $x^U_1 \to x^D_1 \to x^U_2 \to x^D_2$ and $x^U_1 \to x^D_1 \to x^D_3 \to x^U_3$, as shown in Fig. 2. Therefore, the relation of discharge at the interior junction is

$$q(x^U_2) = q(x^D_1) - q(x^D_3), \tag{4}$$

i.e., $\alpha_1 = 0$ and $\alpha_3 = 1$. As a result, the theoretical expression of $q(x^M)$ and $h(x^M)$ at $x^M=\mathcal{V}$ is obtained from Eq. (3):

$$\begin{aligned} \begin{pmatrix} q(x^M) \\ h(x^M) \end{pmatrix} = {} & \mathbf{M}(x^U_2 \to x^M)\left(\mathbf{I}_{22} + (-1)^0\mathbf{I}_{11}\right)\mathbf{M}(x^U_1 \to x^D_1)\begin{pmatrix} q(x^U_1) \\ h(x^U_1) \end{pmatrix} \\ & + \mathbf{M}(x^U_2 \to x^M)(-1)^1\mathbf{I}_{11}\mathbf{M}(x^U_3 \to x^D_3)\begin{pmatrix} q(x^U_3) \\ h(x^U_3) \end{pmatrix} \\ = {} & \mathbf{M}(x^U_2 \to x^M)\mathbf{M}(x^U_1 \to x^D_1)\begin{pmatrix} q(x^U_1) \\ h(x^U_1) \end{pmatrix} \\ & - \mathbf{M}(x^U_2 \to x^M)\mathbf{I}_{11}\mathbf{M}(x^U_3 \to x^D_3)\begin{pmatrix} q(x^U_3) \\ h(x^U_3) \end{pmatrix}. \end{aligned} \tag{5}$$

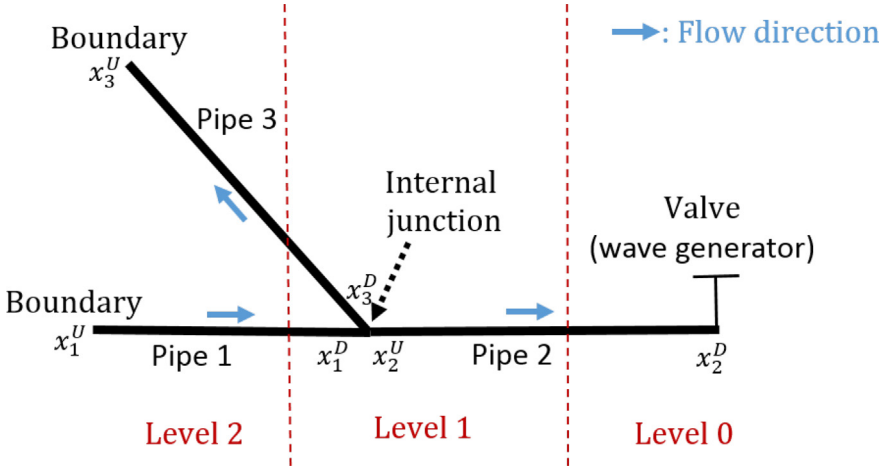

Fig. 2. A network with three pipes.

Example 2. Fig. 3 shows a pipe network with five pipes. In this system, $\partial\mathcal{X}\setminus\mathcal{V}=\{x_3^U,x_4^U,x_5^U\}$ and $\mathcal{V}=\{x_1^D\}$, the three paths from the three boundaries $\partial\mathcal{X}\setminus\mathcal{V}$ to $\mathcal{V}$ are $x_4^U\to x_4^D\to x_2^U\to x_2^D\to x_1^U\to x_1^D, x_5^U\to x_5^D\to x_2^U\to x_2^D\to x_1^U\to x_1^D$, and $x_3^U\to x_3^D\to x_1^U\to x_1^D$. The flow direction is same as the computation path from $\partial\mathcal{X}\setminus\mathcal{V}$ to $\mathcal{V}$. The discharge at the two interior junctions has the relationship:

$$q(x_1^U)=q(x_2^D)+q(x_3^D);\, q(x_2^U)=q(x_4^D)+q(x_5^D), \tag{6}$$

thus $\alpha_2=\alpha_3=\alpha_4=\alpha_5=0$. The discharge and head at $x^M=\mathcal{V}$ can then be computed by

$$\begin{aligned}\begin{pmatrix}q(x^M)\\ h(x^M)\end{pmatrix}= &\ \mathbf{M}(x_1^U\to x^M)\mathbf{M}(x_2^U\to x_2^D)\mathbf{M}(x_4^U\to x_4^D)\begin{pmatrix}q(x_4^U)\\ h(x_4^U)\end{pmatrix}\\ &+\mathbf{M}(x_1^U\to x^M)\mathbf{M}(x_2^U\to x_2^D)\mathbf{I}_{11}\mathbf{M}(x_5^U\to x_5^D)\begin{pmatrix}q(x_5^U)\\ h(x_5^U)\end{pmatrix}\\ &+\mathbf{M}(x_1^U\to x^M)\mathbf{I}_{11}\mathbf{M}(x_3^U\to x_3^D)\begin{pmatrix}q(x_3^U)\\ h(x_3^U)\end{pmatrix}.\end{aligned} \tag{7}$$

2.3. Specific model without and with leak

Here, the transfer matrices in Eq. (3) are specified, which depend on the existence and the location of leak. If there is no leak in the i-th pipe, the transfer matrix is [38]:

$$\mathbf{M}(x_i^U\to x_i^D)=\mathbf{M}^{NL}(x_i^D-x_i^U;A_i), \tag{8}$$

where $A_i=\pi d_i^2/4$ and d_i are respectively the cross-sectional area and the diameter of the i-th pipe,

$$\mathbf{M}^{NL}(x_i;A_i)=\begin{pmatrix}\cosh(\mu_i x_i) & -\frac{1}{Z_i}\sinh(\mu_i x_i)\\ -Z_i\sinh(\mu_i x_i) & \cosh(\mu_i x_i)\end{pmatrix}, \tag{9}$$

$$Z_i(\omega)=\mu_i a_i^2/(\mathrm{i}\omega g A_i) \tag{10}$$

is the characteristic impedance and

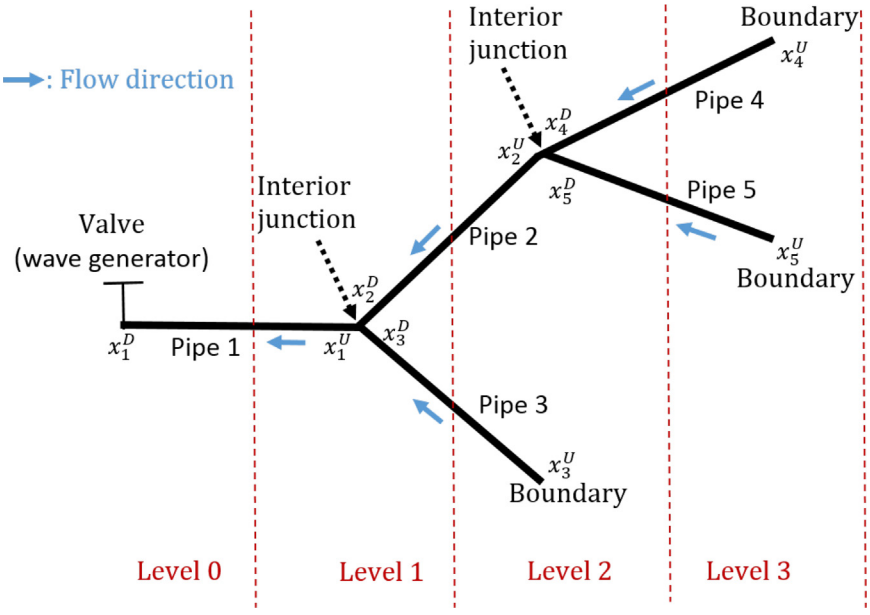

Fig. 3. A pipe network with five pipes.

$$\mu_i(\omega) = a_i^{-1}\sqrt{-\omega^2 + \mathrm{i}gA_i\omega R_i}, \tag{11}$$

is the propagation function, a_i is the wave speed (an introduction of wave speed in elastic and viscoelastic pipes is given in Appendix (A), g is the gravitational acceleration, ω is the angular frequency, and R_i is the steady-state resistance term being $R_i = (f_{DW}Q_{0i})/\left(gd_iA_i^2\right)$ for turbulent flows, in which Q_{0i} is the steady-state discharge in the i-th pipe and f_{DW} is the Darcy–Weisbach friction factor. In this no-leak case, the discharge and head are denoted by q^{NL} and h^{NL} and Eq. (3) becomes

$$\begin{pmatrix} q^{NL}(x^M) \\ h^{NL}(x^M) \end{pmatrix} = \sum_{n=1}^{\mathrm{card}(\partial\mathcal{X}\setminus\mathcal{V})} \mathbf{M}^{NL}\left(x^M - x^U_{n_{p_n}}, A_{n_{p_n}}\right)\left(\prod_{i=p_n-1}^{1} \mathbf{I}^{(n_i)}\mathbf{M}^{NL}\left(x^D_{n_i} - x^U_{n_i}, A_{n_i}\right)\right)\begin{pmatrix} q\left(x^U_{n_1}\right) \\ h\left(x^U_{n_1}\right) \end{pmatrix}. \tag{12}$$

If there is a leak in the i-th pipe where the leak location is x_i^L and the leak size (effective leak orifice area) is s^L, the transfer matrix is [6]:

$$\mathbf{M}(x_i^U \to x_i^D) = \mathbf{M}^{NL}(x_i^D - x_i^U; A_i) + s^L\mathbf{M}^{SL}(x_i^L; A_i, x_i^U, x_i^D), \tag{13}$$

in which

$$\mathbf{M}^{SL}(x_i^L; A_i, x_i^U, x_i^D) = \sqrt{\frac{g}{2\left(H_0^L - z^L\right)}}\begin{pmatrix} Z_i\sinh\left(\mu_i(x_i^L - x_i^U)\right)\cosh\left(\mu_i(x_i^D - x_i^L)\right) & -\cosh\left(\mu_i(x_i^L - x_i^U)\right)\cosh\left(\mu_i(x_i^D - x_i^L)\right) \\ -Z_i^2\sinh\left(\mu_i(x_i^L - x_i^U)\right)\sinh\left(\mu_i(x_i^D - x_i^L)\right) & Z_i\cosh\left(\mu_i(x_i^L - x_i^U)\right)\sinh\left(\mu_i(x_i^D - x_i^L)\right) \end{pmatrix}. \tag{14}$$

Here, z^L denotes the pipe elevation and H_0^L is the steady-state head at the leak. In the presence of a leak, Eq. (13) implies a separation of $(q,h)^\top$ into a term independent of leak, the leak size, and a term dependent only on the leak location. Thus, Eq. (3) has the form:

$$\begin{pmatrix} q(x^M) \\ h(x^M) \end{pmatrix} = \begin{pmatrix} q^{NL}(x^M) \\ h^{NL}(x^M) \end{pmatrix} + s^L\begin{pmatrix} q^*(x^L; x^M) \\ G(x^L; x^M) \end{pmatrix}. \tag{15}$$

In this equation, $q^*(x^L; x^M)$ and $G(x^L; x^M)$ are functions of leak location x^L but independent of leak size s^L; its explicit form depends on the topology of the network and is illustrated using the following examples. In this paper, the head $h(x^M)$ is measured and used to estimate the leak location x^L and size s^L; by the second line of Eq. (15), $h(x^M)$ has the theoretical expression

$$h(x^M) = h^{NL}(x^M) + s^L G(x^L; x^M). \tag{16}$$

Example 3. Here, the pipe network in Example 1 is further studied, where the system is shown in Fig. 2. In the case of no leak, the discharge and head at x^M are obtained by inserting Eq. (8) into Eq. (5):

$$\begin{pmatrix} q^{NL}(x^M) \\ h^{NL}(x^M) \end{pmatrix} = \mathbf{M}^{NL}(x^M - x_2^U; A_2)\mathbf{M}^{NL}(x_1^D - x_1^U; A_1)\begin{pmatrix} q(x_1^U) \\ h(x_1^U) \end{pmatrix} - \mathbf{M}^{NL}(x^M - x_2^U; A_2)\mathbf{I}_{11}\mathbf{M}^{NL}(x_3^D - x_3^U; A_3)\begin{pmatrix} q(x_3^U) \\ h(x_3^U) \end{pmatrix}. \tag{17}$$

When one leak exists in Pipe 1,

$$\begin{cases} \mathbf{M}(x_1^U \to x_1^D) = \mathbf{M}^{NL}(x_1^D - x_1^U; A_1) + s^L\mathbf{M}^{SL}(x_1^L; A_1, x_1^U, x_1^D) \\ \mathbf{M}(x_2^U \to x_2^M) = \mathbf{M}^{NL}(x_2^M - x_2^U; A_2) \\ \mathbf{M}(x_3^U \to x_3^D) = \mathbf{M}^{NL}(x_3^D - x_3^U; A_3) \end{cases}, \tag{18}$$

and

$$\begin{pmatrix} q(x^M) \\ h(x^M) \end{pmatrix} = \begin{pmatrix} q^{NL}(x^M) \\ h^{NL}(x^M) \end{pmatrix} + s^L\mathbf{M}^{NL}(x^M - x_2^U; A_2)\mathbf{M}^{SL}(x_1^L; A_1, x_1^U, x_1^D)\begin{pmatrix} q(x_1^U) \\ h(x_1^U) \end{pmatrix}. \tag{19}$$

In the case of one leak in Pipe 2, the transfer matrices are

$$\begin{cases} \mathbf{M}(x_1^U \to x_1^D) = \mathbf{M}^{NL}(x_1^D - x_1^U; A_1) \\ \mathbf{M}(x_2^U \to x^M) = \mathbf{M}^{NL}(x^M - x_2^U; A_2) + s^L\mathbf{M}^{SL}(x_2^L; A_2, x_2^U, x^M) \\ \mathbf{M}(x_3^U \to x_3^D) = \mathbf{M}^{NL}(x_3^D - x_3^U; A_3) \end{cases}. \tag{20}$$

Therefore,

$$\begin{pmatrix} q(x^M) \\ h(x^M) \end{pmatrix} = \begin{pmatrix} q^{NL}(x^M) \\ h^{NL}(x^M) \end{pmatrix} + s^L \mathbf{M}^{SL}(x_2^L; A_2, x_2^U, x^M) \left[\mathbf{M}^{NL}(x_1^D - x_1^U; A_1) \begin{pmatrix} q(x_1^U) \\ h(x_1^U) \end{pmatrix} - \mathbf{I}_{11} \mathbf{M}^{NL}(x_3^D - x_3^U; A_3) \begin{pmatrix} q(x_3^U) \\ h(x_3^U) \end{pmatrix} \right]. \tag{21}$$

In the case of one leak in Pipe 3, the transfer matrices are

$$\begin{cases} \mathbf{M}(x_1^U \to x_1^D) = \mathbf{M}^{NL}(x_1^D - x_1^U; A_1) \\ \mathbf{M}(x_2^U \to x^M) = \mathbf{M}^{NL}(x^M - x_2^U; A_2) \\ \mathbf{M}(x_3^U \to x_3^D) = \mathbf{M}^{NL}(x_3^D - x_3^U; A_3) + s^L \mathbf{M}^{SL}(x_3^L; A_3, x_3^U, x_3^D) \end{cases}. \tag{22}$$

In this case,

$$\begin{pmatrix} q(x^M) \\ h(x^M) \end{pmatrix} = \begin{pmatrix} q^{NL}(x^M) \\ h^{NL}(x^M) \end{pmatrix} - s^L \mathbf{M}^{NL}(x^M - x_2^U; A_2) \mathbf{I}_{11} \mathbf{M}^{SL}(x_3^L; A_3, x_3^U, x_3^D) \begin{pmatrix} q(x_3^U) \\ h(x_3^U) \end{pmatrix}. \tag{23}$$

By expanding Eqs. (17), (19), (21), and (23), the head at x^M follows Eq. (16). The explicit forms of $h^{NL}(x^M)$ and $G(x^L; x^M)$ in this equation are given in Appendix B.

Example 4. Here, the pipe network in Fig. 3 and Example 2 is further studied. In the case of no leak, the discharge and head in Eq. (7) become

$$\begin{aligned} \begin{pmatrix} q^{NL}(x^M) \\ h^{NL}(x^M) \end{pmatrix} &= \mathbf{M}^{NL}(x^M - x_1^U; A_1) \mathbf{M}^{NL}(x_2^D - x_2^U; A_2) \mathbf{M}^{NL}(x_4^D - x_4^U; A_4) \begin{pmatrix} q(x_4^U) \\ h(x_4^U) \end{pmatrix} \\ &+ \mathbf{M}^{NL}(x^M - x_1^U; A_1) \mathbf{M}^{NL}(x_2^D - x_2^U; A_2) \mathbf{I}_{11} \mathbf{M}^{NL}(x_5^D - x_5^U; A_5) \begin{pmatrix} q(x_5^U) \\ h(x_5^U) \end{pmatrix} \\ &+ \mathbf{M}^{NL}(x^M - x_1^U; A_1) \mathbf{I}_{11} \mathbf{M}^{NL}(x_3^D - x_3^U; A_3) \begin{pmatrix} q(x_3^U) \\ h(x_3^U) \end{pmatrix}. \end{aligned} \tag{24}$$

In the case of one leak x_1^L in Pipe 1,

$$\begin{aligned} \begin{pmatrix} q(x^M) \\ h(x^M) \end{pmatrix} &= \begin{pmatrix} q^{NL}(x^M) \\ h^{NL}(x^M) \end{pmatrix} + s^L \mathbf{M}^{SL}(x_1^L; A_1, x_1^U, x^M) \mathbf{M}^{NL}(x_2^D - x_2^U; A_2) \mathbf{M}^{NL}(x_4^D - x_4^U; A_4) \begin{pmatrix} q(x_4^U) \\ h(x_4^U) \end{pmatrix} \\ &+ s^L \mathbf{M}^{SL}(x_1^L; A_1, x_1^U, x^M) \mathbf{M}^{NL}(x_2^D - x_2^U; A_2) \mathbf{I}_{11} \mathbf{M}^{NL}(x_5^D - x_5^U; A_5) \begin{pmatrix} q(x_5^U) \\ h(x_5^U) \end{pmatrix} \\ &+ s^L \mathbf{M}^{SL}(x_1^L; A_1, x_1^U, x^M) \mathbf{I}_{11} \mathbf{M}^{NL}(x_3^D - x_3^U; A_3) \begin{pmatrix} q(x_3^U) \\ h(x_3^U) \end{pmatrix}. \end{aligned} \tag{25}$$

In the case of one leak x_2^L in Pipe 2,

$$\begin{aligned} \begin{pmatrix} q(x^M) \\ h(x^M) \end{pmatrix} &= \begin{pmatrix} q^{NL}(x^M) \\ h^{NL}(x^M) \end{pmatrix} + s^L \mathbf{M}^{NL}(x^M - x_1^U; A_1) \mathbf{M}^{SL}(x_2^L; A_2, x_2^U, x_2^D) \mathbf{M}^{NL}(x_4^D - x_4^U; A_4) \begin{pmatrix} q(x_4^U) \\ h(x_4^U) \end{pmatrix} \\ &+ s^L \mathbf{M}^{NL}(x^M - x_1^U; A_1) \mathbf{M}^{SL}(x_2^L; A_2, x_2^U, x_2^D) \mathbf{I}_{11} \mathbf{M}^{NL}(x_5^D - x_5^U; A_5) \begin{pmatrix} q(x_5^U) \\ h(x_5^U) \end{pmatrix}. \end{aligned} \tag{26}$$

In the case of one leak x_3^L in Pipe 3,

$$\begin{pmatrix} q(x^M) \\ h(x^M) \end{pmatrix} = \begin{pmatrix} q^{NL}(x^M) \\ h^{NL}(x^M) \end{pmatrix} + s^L \mathbf{M}^{NL}(x^M - x_1^U; A_1) \mathbf{I}_{11} \mathbf{M}^{SL}(x_3^L; A_3, x_3^U, x_3^D) \begin{pmatrix} q(x_3^U) \\ h(x_3^U) \end{pmatrix}. \tag{27}$$

In the case of one leak x_4^L in Pipe 4,

$$\begin{pmatrix} q(x^M) \\ h(x^M) \end{pmatrix} = \begin{pmatrix} q^{NL}(x^M) \\ h^{NL}(x^M) \end{pmatrix} + s^L \mathbf{M}^{NL}(x^M - x_1^U; A_1) \mathbf{M}^{NL}(x_2^D - x_2^U; A_2) \mathbf{M}^{SL}(x_4^L; A_4, x_4^U, x_4^D) \begin{pmatrix} q(x_4^U) \\ h(x_4^U) \end{pmatrix}. \tag{28}$$

In the case of one leak x_5^L in Pipe 5,

$$\begin{pmatrix} q(x^M) \\ h(x^M) \end{pmatrix} = \begin{pmatrix} q^{NL}(x^M) \\ h^{NL}(x^M) \end{pmatrix} + s^L \mathbf{M}^{NL}(x^M - x_1^U; A_1) \mathbf{M}^{NL}(x_2^D - x_2^U; A_2) \mathbf{I}_{11} \mathbf{M}^{SL}(x_5^L; A_5, x_5^U, x_5^D) \begin{pmatrix} q(x_5^U) \\ h(x_5^U) \end{pmatrix}. \tag{29}$$

Similar to Example 3, Eq. (16) and $G(x^L;x^M)$ for this five-pipe network can be obtained by the second lines of the above six equations.

2.4. Boundary condition

In this paper, the leakage estimation is realized by matching the head measurement with its theoretical model Eq. (16) to decide the optimal x^L and s^L. For this purpose, as can be seen from the right hand side of Eq. (16), the boundary conditions $h\left(x^U_{n_1}\right)$ and $q\left(x^U_{n_1}\right)$ at each boundary of the network $x^U_{n_1}\in\partial\mathcal{X}/\mathcal{V}$ are needed. Here, three situations of the boundary at $x^U_{n_1}$ are discussed and the corresponding boundary conditions are obtained.

- **Case I**: If $x^U_{n_1}$ is a reservoir or a centrifugal pump, the boundary condition

$$h\left(x^U_{n_1}\right)=0 \tag{30}$$

can be assumed. Furthermore, a sensor is set near $x^U_{n_1}$ whose location is denoted by $x^M_{n_1}$ and it is assumed that there is no leak between $x^U_{n_1}$ and $x^M_{n_1}$. Then, $q\left(x^U_{n_1}\right)$ can be estimated [46,47,24] by

$$\hat{q}\left(x^U_{n_1}\right)=\frac{\cosh\left(\mu_{n_1}\left(x^M_{n_1}-x^U_{n_1}\right)\right)h\left(x^U_{n_1}\right)-h\left(x^M_{n_1}\right)}{Z_{n_1}\sinh\left(\mu_{n_1}\left(x^M_{n_1}-x^U_{n_1}\right)\right)} \tag{31}$$

$$=-\frac{h\left(x^M_{n_1}\right)}{Z_{n_1}\sinh\left(\mu_{n_1}\left(x^M_{n_1}-x^U_{n_1}\right)\right)}. \tag{32}$$

- **Case II**: If $x^U_{n_1}$ is a dead-end,

$$q\left(x^U_{n_1}\right)=0. \tag{33}$$

As the previous case, $h\left(x^M_{n_1}\right)$ is measured at $x^M_{n_1}$. By solving

$$\begin{pmatrix} q\left(x^U_{n_1}\right)\\ h\left(x^U_{n_1}\right)\end{pmatrix}=\mathbf{M}^{NL}\left(x^U_{n_1}-x^M_{n_1};A_{n_1}\right)\begin{pmatrix} q\left(x^M_{n_1}\right)\\ h\left(x^M_{n_1}\right)\end{pmatrix}, \tag{34}$$

we have

$$\hat{h}\left(x^U_{n_1}\right)=\frac{Z_{n_1}\sinh\left(\mu_{n_1}\left(x^U_{n_1}-x^M_{n_1}\right)\right)q\left(x^U_{n_1}\right)+h\left(x^M_{n_1}\right)}{\cosh\left(\mu_{n_1}\left(x^U_{n_1}-x^M_{n_1}\right)\right)}=\frac{h\left(x^M_{n_1}\right)}{\cosh\left(\mu_{n_1}\left(x^U_{n_1}-x^M_{n_1}\right)\right)}. \tag{35}$$

- **Case III**: For a dynamic boundary which is not well-defined and both Eqs. (30) and (33) cannot be applied, additional sensors are required. It is necessary to measure both $h\left(x^U_{n_1}\right)$ and $h\left(x^M_{n_1}\right)$; then, $q\left(x^U_{n_1}\right)$ is estimated via Eq. (31).

If all the boundaries follow Eqs. (30) or (33) (Case I or II), $\mathrm{card}(\partial\mathcal{X}\setminus\mathcal{V})$ sensors are needed to obtain the boundary conditions and in total $\mathrm{card}(\partial\mathcal{X}\setminus\mathcal{V})+1$ sensors are needed for leakage estimation (detailed in Section 3). For any boundary in $\partial\mathcal{X}\setminus\mathcal{V}$ where both Eqs. (30) and (33) cannot be assumed (i.e., Case III), an additional sensor has to be added for estimating the boundary conditions. In short, no more than $2\mathrm{card}(\partial\mathcal{X}\setminus\mathcal{V})+1$ sensors are required for the leak localization method proposed in this paper.

3. Leak estimation scheme

In this section, the head differences from a sensor located at x^M with K frequencies, denoted as $\Delta\mathbf{h}=(\Delta h_1,\ldots,\Delta h_K)^\top$, are used to estimate the leak location x^L and size s^L. Here,

$$\Delta h_k=h(x^M,\omega_k)-h^{NL}(x^M,\omega_k),\quad k=1,\ldots,K. \tag{36}$$

In practice, $h(x^M,\omega_k)$ is measured and $h^{NL}(x^M,\omega_k)$ is obtained from the transient model for the case with no leak in Eq. (12). We denote

$$\mathbf{G}(x^L) = \left(G(x^L; x^M, \omega_1), \ldots, G(x^L; x^M, \omega_K)\right)^\top, \tag{37}$$

which is a function of the leak location $x^L \in \mathcal{X}$. Considering an additive noise vector $\mathbf{n} = (n_1, \ldots, n_K)^\top$, then the head difference has the theoretical expression

$$\Delta\mathbf{h} = s^L \mathbf{G}(x^L) + \mathbf{n}. \tag{38}$$

The noise vector $\mathbf{n}$ is assumed to follow the zero-mean Gaussian distribution $\mathcal{N}(\mathbf{0}, \sigma^2\mathbf{I}_K)$, where $\mathbf{I}_K$ is the K-dimensional identity matrix. For a general covariance matrix of $\mathbf{n}$, a data transformation technique for noise whitening [6,48] can be applied such that the independent white noise assumption still holds.

Then, the leakage localization problem is solved using the MFP method [6,25]. The leak location and size are estimated, separately and sequentially, as

$$\widehat{x^L} = \arg\max_{x^L \in \mathcal{X}} \frac{\Delta\mathbf{h}^H \mathbf{G}(x^L)\mathbf{G}^H(x^L)\Delta\mathbf{h}}{\mathbf{G}^H(x^L)\mathbf{G}(x^L)} \tag{39}$$

and

$$\widehat{s^L} = \frac{\mathbf{G}^H\left(\widehat{x^L}\right)\Delta\mathbf{h}}{\mathbf{G}^H\left(\widehat{x^L}\right)\mathbf{G}\left(\widehat{x^L}\right)}. \tag{40}$$

The derivation of Eqs. (39) and (40) is based on the MFP principle [6] and is recalled in Appendix C. Eq. (39) implies that the leak is localized by a 1D search of leak location along all the pipes in the network. Since $\mathbf{G}$ is analytical and $\mathcal{X}$ is a 1D network, the proposed method does not need any optimization technique, but just plots the 1D analytical objective function in Eq. (39) throughout $\mathcal{X}$, thus the computation is very fast.

Finally, the MFP algorithm of leakage localization in a tree-structured pipe network is summarized in Algorithm 1.

Algorithm 1. Leak localization in a tree-type pipe network using MFP

1. Select K frequencies $\omega_1, \ldots, \omega_K$.
2. Obtain the boundary conditions $h\left(x^U_{n_1}, \omega_k\right)$ from Eqs. (30) or (35) and $q\left(x^U_{n_1}, \omega_k\right)$ from Eqs. (32) or (33) for each $x^U_{n_1} \in \partial\mathcal{X} \setminus \mathcal{V}$.
3. Calculate $h^{NL}(x^M, \omega_k)$ via Eq. (12) and use the head differences $\Delta\mathbf{h}$ (Eq. (38)) as the data.
4. Plot the objective function in Eq. (39):
   $|B|^2 = \frac{\Delta\mathbf{h}^H \mathbf{G}(x^L)\mathbf{G}^H(x^L)\Delta\mathbf{h}}{\mathbf{G}^H(x^L)\mathbf{G}(x^L)}$. (41)
   with respect to $x^L \in \mathcal{X}$ along the whole network (discretizing Eq. (41) with a spatial grid size lower than half minimum wavelength) and retain x^L corresponding to maximum $|B|^2$ as the leak location estimate.
5. Estimate the leak size via Eq. (40).

4. Numerical simulation

In this section, the three-pipe and five-pipe examples are revisited; the proposed leakage localization method is tested numerically.

4.1. Three-pipe network

4.1.1. Setup, measured signal, and leak localization using MFP

In this section, we introduce numerical results of leak estimation in the three-pipe system in Fig. 2 and Examples 1 and 3. The numerical setup of the system with more details is shown in Fig. 4. The lengths of the three pipes are $l_1 = 600$ m, $l_2 = 500$ m, and $l_3 = 400$ m; the diameters are $d_1 = 0.5$ m, $d_2 = 0.5$ m, and $d_3 = 0.4$ m, respectively. The coordinate system for the three pipes is: $x \in [x_i^U, x_i^D]$ in the i-th pipe ($i = 1, 2, 3$), where $x_1^U = 0, x_1^D = x_2^U = x_3^D = l_1 = 600$ m, $x_2^D = l_1 + l_2 = 1100$ m and $x_3^U = l_1 + l_3 = 1000$ m. The steady-state head at the upstream reservoir is $H_1 = 25$ m. The pipe material is elastic and the wave speed is $a = 1000$ m/s. The Darcy–Weisbach friction factor is $f_{DW} = 0.02$. Three measurement stations are respectively located in the three pipes: $x_1^M = 50$ m in Pipe 1, $x_2^M = 1100$ m in Pipe 2, and $x_3^M = 920$ m in Pipe 3.

The transient wave is generated by a sudden closure of the valve at x_2^D. A leak is located at $x_3^L = 760$ m in Pipe 3 and the leak size is $s^L = 3 \times 10^{-4}$ m^2. The wave propagation is simulated via the method of characteristics (MOC) [38]. Fig. 5(a) shows

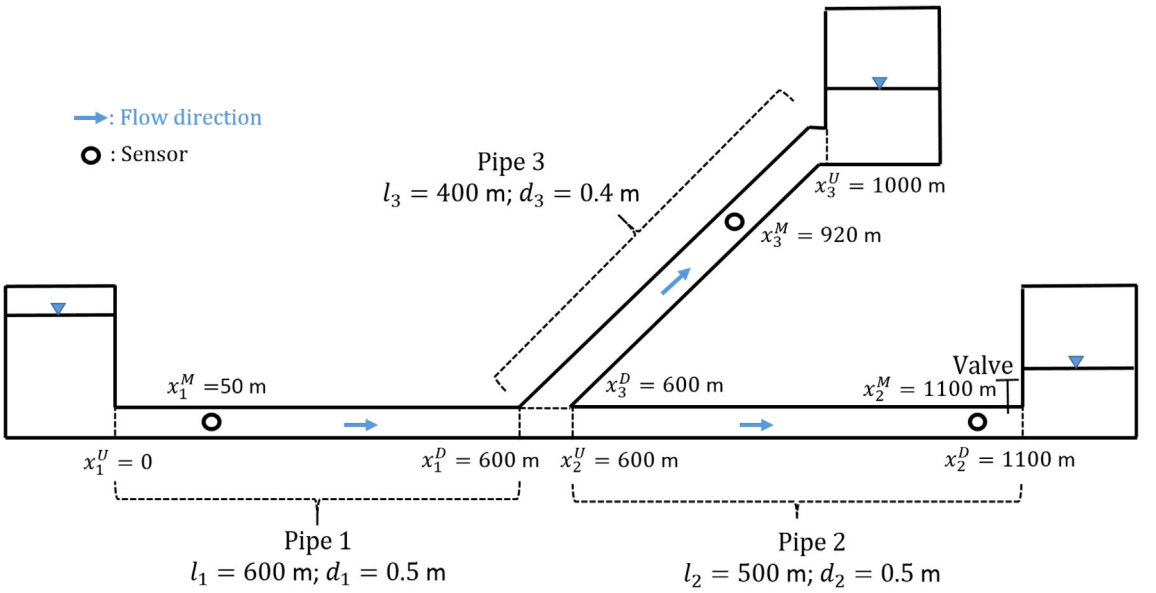

Fig. 4. Setup of the pipe network with three pipes considered in the numerical examples in Section 4.1.

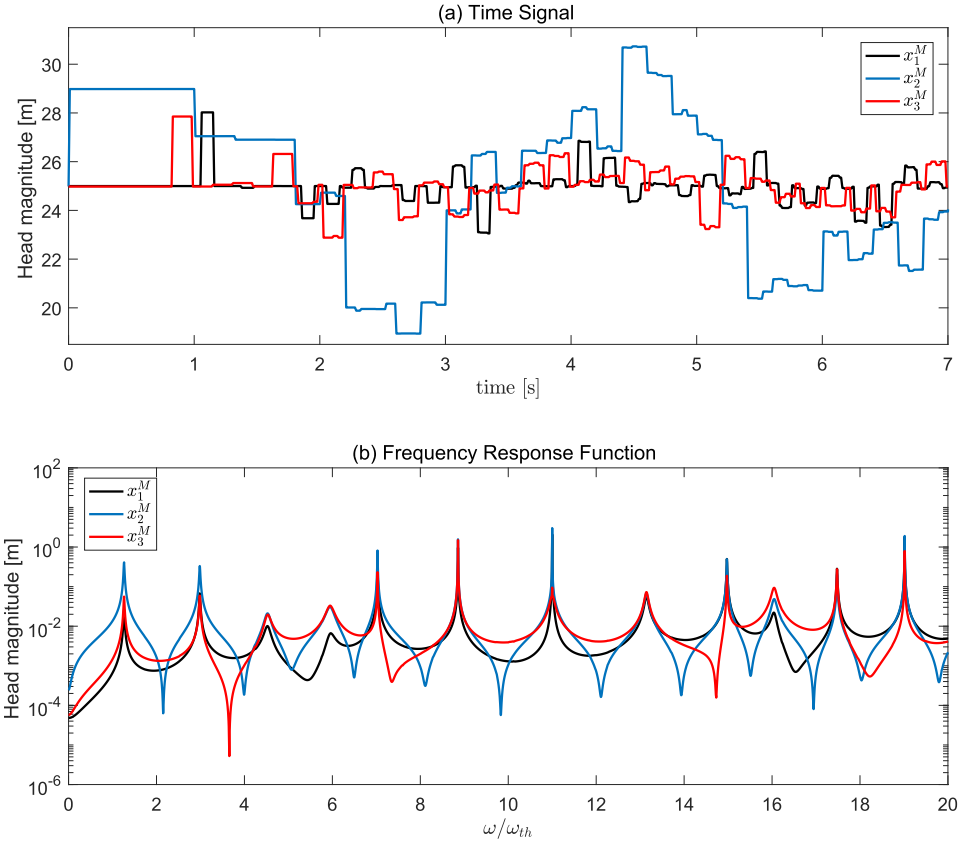

Fig. 5. (a) Time signals (simulated via MOC) and (b) FRFs at x_1^M, x_2^M, and x_3^M. A single leak is located at $x_3^l = 760$ m in Pipe 3.

the time signals at the three measurement stations. The FRFs (normalized by $\omega_{th} = a\pi/(2(l_1 + l_2))$) are computed from the time signals in Fig. 5(a) [25,42] and are shown in Fig. 5(b). The frequencies used for leakage detection are $\{\omega : \omega/\omega_{th} = 0.01, 0.02, \ldots, 20\}$; the maximum frequency is 4.5 Hz and the minimum wavelength is 222 m. The leak local-

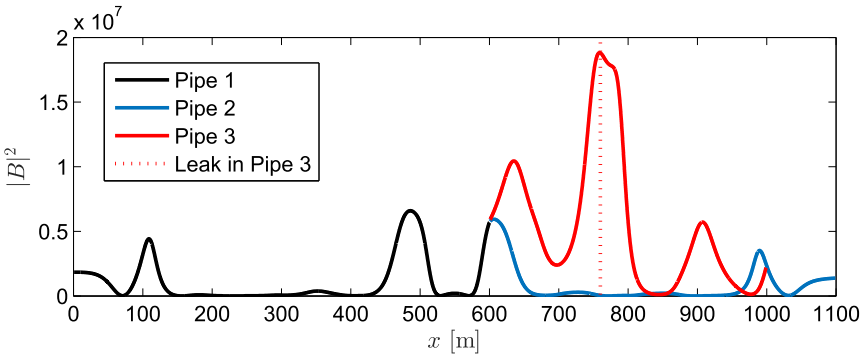

Fig. 6. Single leak localization using MFP by plotting $|B|^2$ along the three pipes. A single leak is located at $x_3^L = 760$ m in Pipe 3 (160 m from the junction); its actual location is represented by the vertical dotted line.

ization is implemented using MFP by plotting $|B|^2$ along the three pipes, as shown in Fig. 6. The leak location estimate is $\widehat{x_3^L} = 759$ m in Pipe 3, i.e., the error is 1 m, and the leak size estimate is $\widehat{s^L} = 2.92 \times 10^{-4}$ m^2 (the relative error is 2.67%). Here, the signal used for leak localization is free of noise, but slight modeling error is introduced since the simulated data are generated by the time-domain numerical MOC model whereas the MFP leak estimation uses the frequency-domain model which linearizes the orifice equation and the turbulent friction term in the momentum equation [38]. In Section 4.1.2, artificial noise is further added to the simulated data in Fig. 5 to evaluate the performance of the proposed leakage detection method in noisy environments.

4.1.2. Performance analysis in noisy environments and comparison with the methods in the literature

In this section, the MFP is compared with two representative methods in the literature:

- Wavelet transform analysis (WTA) method [28]: The mother wavelet is the type Daubechies of order 1 (db1). It analyzes the drop due to leak by picking the maximum reflection (sudden change in the measured signal) after excluding the reflections from boundaries and junctions and, then, decides the leak-sensor distance.

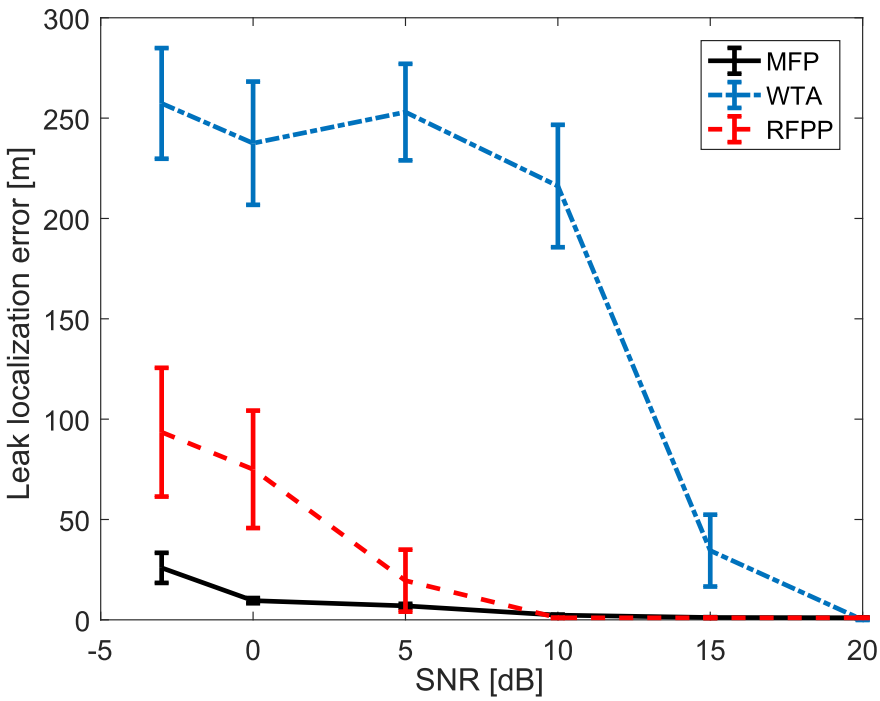

Fig. 7. Average and 95% confidence interval of leak localization error using MFP, WTA and RFPP.

- Resonant frequency peak pattern (RFPP) of FRF [31]: The first ten resonant frequency peaks are used. The leak is searched in all the three pipes.

The leak localization error is 0 m for WTA and 1 m for RFPP if the signals in Fig. 5 (without additional noise) are used.

Then, Gaussian-distributed random noise with zero-mean and standard deviation σ is added to the time signal in Fig. 5 (a); the signal-to-noise ratio (SNR) in dB is defined as [26]:

$$\mathrm{SNR} = 20\log_{10}(|h_{drop}|/\sigma). \tag{42}$$

Here, h_{drop} is the head drop at the first leak reflection. In this case where the leak size is $s^L = 3 \times 10^{-4}$ m^2, $h_{drop} = 0.15$ m. The time signal after adding noise is then transfered to FRF.

The leak localization is tested with different SNR from -3 dB to 20 dB. For each SNR, the procedure from data simulation to leak localization is repeated 30 times. The average leak localization errors, as well as the 95% confidence intervals of leak localization error, using the MFP, WTA and RFPP methods are shown in Fig. 7. WTA perfectly localizes the leak (the error is 0 m) when SNR $\geqslant$ 20 dB but is sensitive to stronger noise (SNR $\leqslant$ 15 dB). MFP is the most robust method for low SNR. Here, RFPP considers only the resonant frequencies but MFP uses all the frequencies in the same frequency range and, thus, more robust to noise. Note that, in real pipe networks, the mismatch between the measurement and the model originates from not only the random noise, but also the modeling error due to imprecise knowledge about the system [49]. The numerical noise tests in this section partially illustrate the robustness of the proposed method, but more tests in various experimental environments are further needed.

4.1.3. Detectability of one leak and two leaks

One leak located in different pipes of the network is considered. Gaussian random noise with SNR = 10 dB is added in each case. Fig. 8 shows the MFP localization result of a single leak where $x_1^L = 240$ m in Pipe 1 and $x_2^L = 800$ m in Pipe 2 (200 m from the interior junction), respectively. It is clear that a single leak in any pipe can be accurately localized.

Furthermore, localization of two leaks using the proposed MFP method is analyzed. It is emphasized that, here, the single-leak model (Eq. (38)) is used to localize multiple leaks. This is possible due to the linear superposition property of contributions from various leaks to the MFP objective function; a more detailed introduction for this issue can be found in [6]. In this

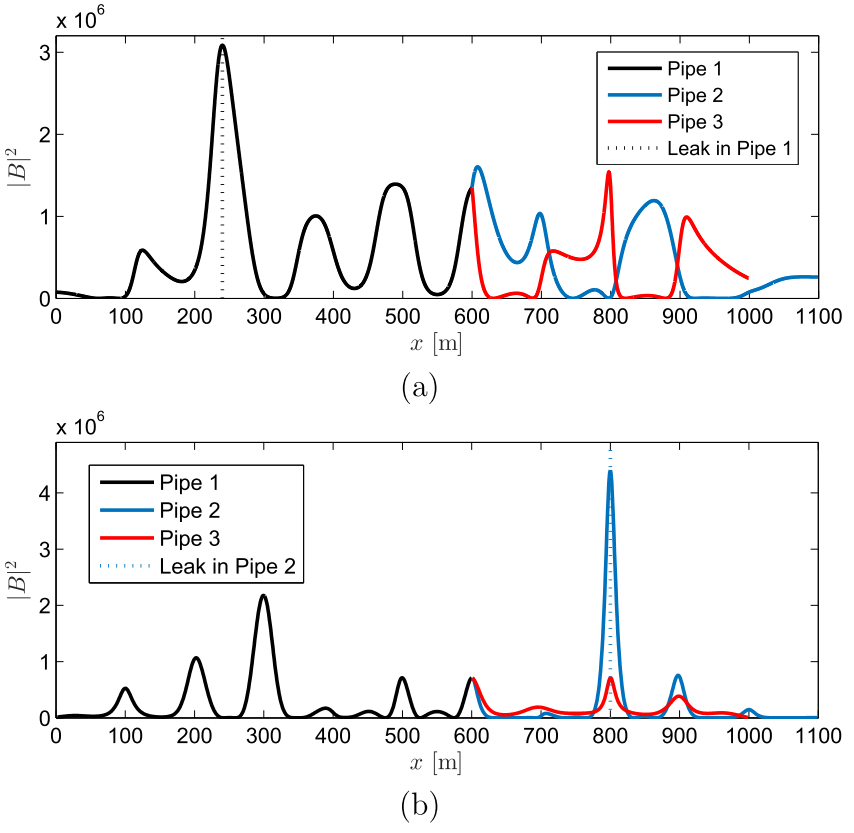

Fig. 8. Single leak localization using MFP by plotting $|B|^2$ along the three pipes. A single leak is located at (a) $x_1^L = 240$ m in Pipe 1 and (b) $x_2^L = 800$ m in Pipe 2. The actual location is represented by the vertical dotted line.

section, the following seven cases with different leak locations are considered (the corresponding MFP leakage localization results are shown in Figs. 9 and 10):

- **Case a** (Fig. 9(a)): Two leaks both in Pipe 1 at $x_1^{L1} = 120$ m and $x_1^{L2} = 240$ m, respectively.
- **Case a'** (Fig. 9(b)): Two leaks both in Pipe 1 at $x_1^{L1} = 120$ m and $x_1^{L2} = 150$ m, respectively.
- **Case b** (Fig. 9(c)): Two leaks both in Pipe 2 at $x_2^{L1} = 750$ m and $x_2^{L2} = 900$, respectively.
- **Case c** (Fig. 9(d)): Two leaks both in Pipe 3 at $x_3^{L1} = 840$ m and $x_3^{L2} = 960$, respectively.

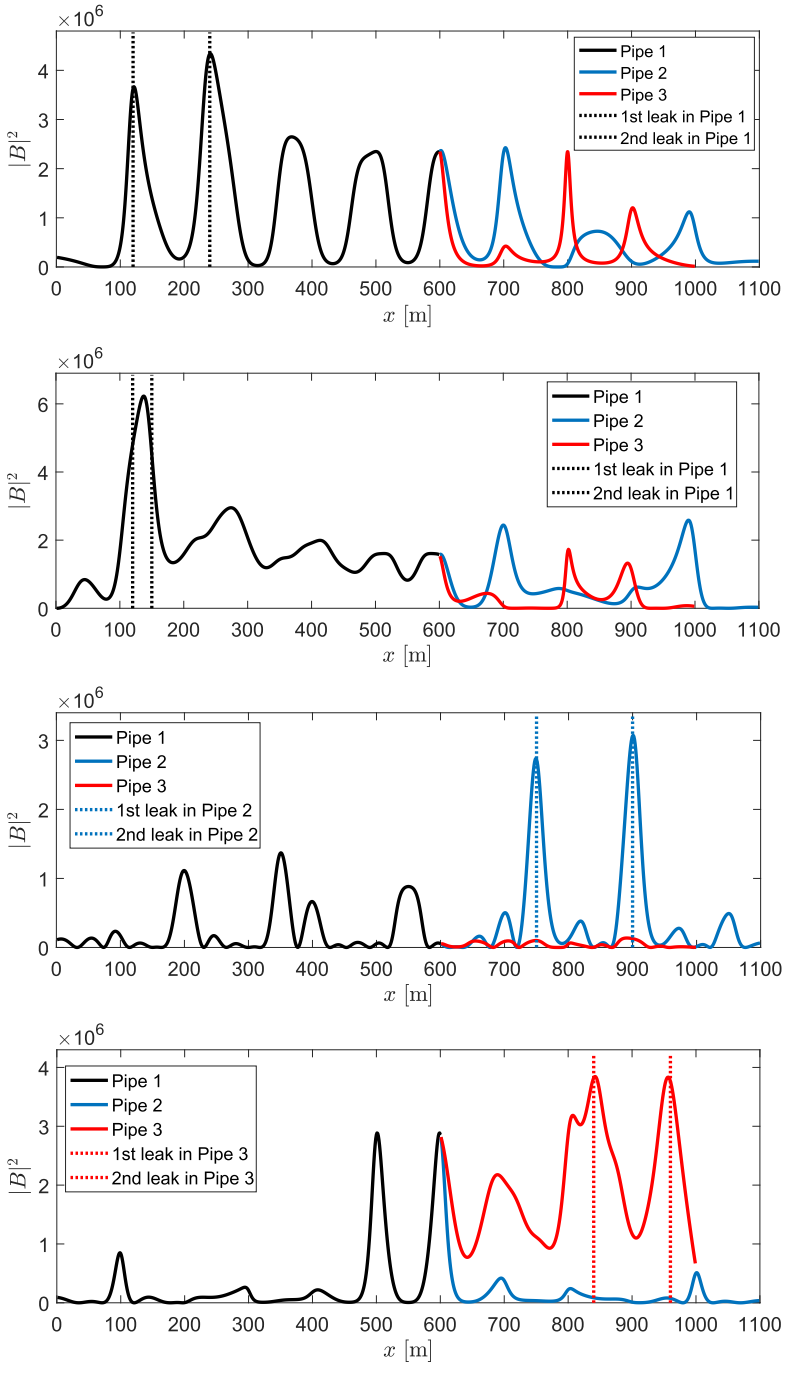

Fig. 9. Localization of two leaks in a same pipe using MFP by plotting $|B|^2$ along the three pipes. The actual leak locations are represented by the vertical dotted lines.

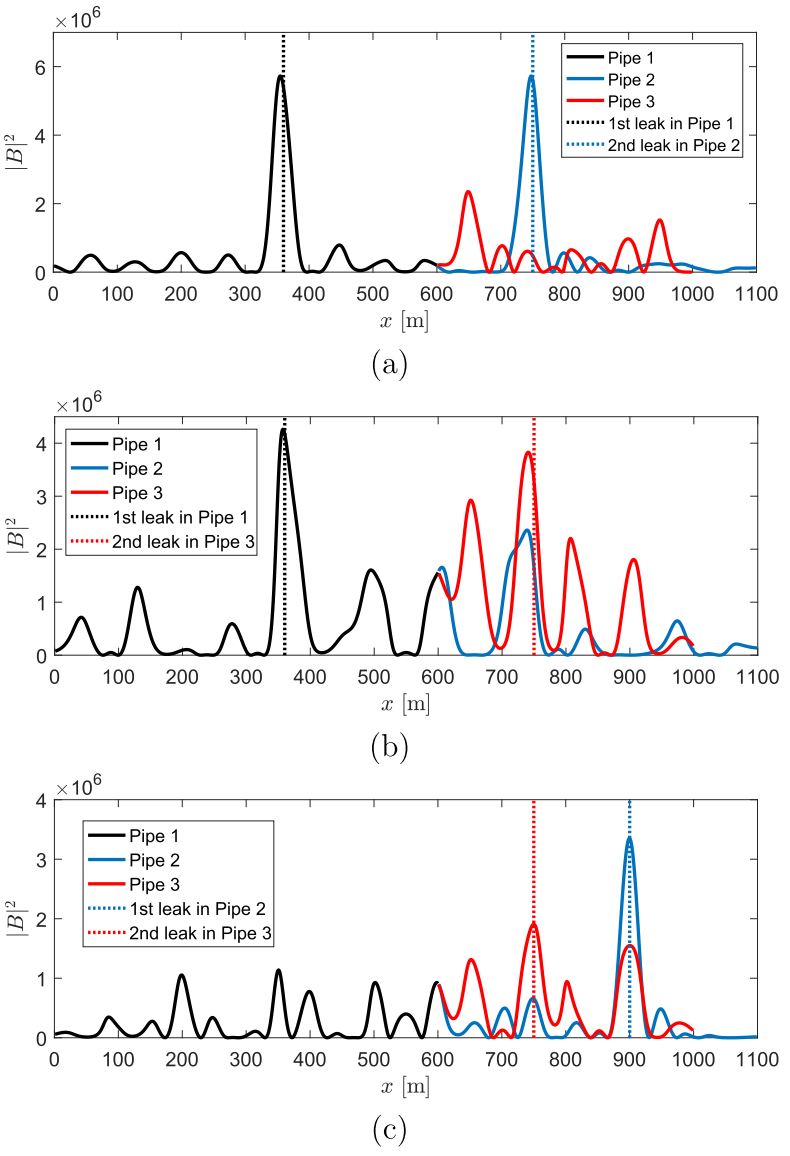

Fig. 10. Localization of two leaks in different pipes using MFP by plotting $|B|^2$ along the three pipes. The actual leak locations are represented by the vertical dotted lines.

- **Case d** (Fig. 10(a)): Two leaks located at $x_1^{L1} = 360$ m in Pipe 1 and $x_2^{L2} = 750$ m in Pipe 2, respectively.
- **Case e** (Fig. 10(b)): Two leaks located at $x_1^{L1} = 360$ m in Pipe 1 and $x_3^{L2} = 750$ m in Pipe 3, respectively.
- **Case f** (Fig. 10(c)): Two leaks located at $x_2^{L1} = 900$ m in Pipe 2 and $x_3^{L2} = 750$ m in Pipe 3, respectively.

Note that in Case a, the distance between the two leaks (120 m) is higher than half minimum wavelength, being $\lambda_{\min}/2 = \pi a/\omega_{\max} = 111$ m. In this case, two leaks can be separately and accurately identified. However, in Case a' where two leaks are located in the same pipe as Case a, only one peak of the MFP objective function appears between the two actual leaks. This is because, in Case a', the distance between the two leaks ($|x_1^{L1} - x_1^{L2}| = 30$ m) is lower than $\lambda_{\min}/2 = 111$m (resolvable distance of MFP given this probing transient wave). This result is consistent with the Nyquist-Shannon sampling theorem and previous findings regarding the resolution of the MFP method in a single pipe [6,24].

Fig. 9(c) and (d) show that two leaks in any pipe can be localized. Fig. 10 illustrates that two leaks in different branches can also be localized. In practice, however, the leak number in the system is unknown, the MFP method cannot fully decide all the leaks. As a matter of fact, as indicated in [6,26], the 1D leak search using MFP can only guarantee the existence of a significant peak of MFP objective function near an actual leak. Similar to the previous works for a single pipe [24,50,51], a more elaborated model that parameterizes multiple leaks, as well as the corresponding inverse techniques that can deal with

more parameters, is needed to fully decide the number and the locations of multiple leaks in a pipe network. This issue is beyond the scope of the present paper.

4.2. Five-pipe network

In this section, the five-pipe network in Examples 2 and 4 and Fig. 3 are revisited. The numerical setup of the pipe network with more details is shown in Fig. 11. The lengths of the five pipes are $l_1 = 500$ m, $l_2 = 500$ m, $l_3 = 400$ m, $l_4 = 500$ m, and $l_5 = 400$ m; the diameters are $d_i = 0.5$ m, $i = 1, \ldots, 5$. The coordinate system for the network is: in Pipe 1, $x \in [x_1^U, x_1^D]$ where $x_1^U = 1000$ m and $x_1^D = 1500$ m; in Pipe 2, $x \in [x_2^U, x_2^D]$ where $x_2^U = 500$ m and $x_2^D = 1000$ m; in Pipe 3, $x \in [x_3^U, x_3^D]$ where $x_3^U = 600$ m and $x_3^D = 1000$ m; in Pipe 4, $x \in [x_4^U, x_4^D]$ where $x_4^U = 0$ m and $x_4^D = 500$ m; in Pipe 5, $x \in [x_5^U, x_5^D]$ where $x_5^U = 100$ m and $x_5^D = 500$ m. The pipe material is elastic and the wave speed is $a = 1000$ m/s. The Darcy–Weisbach friction factor is $f_{DW} = 0.02$. The steady-state head at the upstream reservoir x_4^U is $H(x_4^U) = 25$ m. Four measurement stations are located in each of four pipes: $x_1^M = 1500$ m (at the valve) in Pipe 1, $x_3^M = 650$ m in Pipe 3, $x_4^M = 50$ m in Pipe 4, and $x_5^M = 150$ m in Pipe 5.

The transient wave is generated at x_1^D. The frequencies used for leakage detection is $\{\omega : \omega/\omega_{th} = 0.2, 0.4, \ldots, 20\}$, where $\omega_{th} = a\pi/(2(l_1 + l_2 + l_4))$. The leak localization is implemented using MFP by plotting $|B|^2$ along the five pipes. Five cases of single leak are considered; the leak is located at $x_1^L = 1200$ m in Pipe 1, $x_2^L = 600$ m in Pipe 2, $x_3^L = 900$ m in Pipe 3, $x_4^L = 200$ m in Pipe 4, and $x_5^L = 200$ m in Pipe 5. The leak size is $s^L = 1.4 \times 10^{-4}$ m^2. The SNR is 10 dB. The results of single leak localization with the five cases of leak location are shown in Fig. 12, which demonstrates that the leak can be accurately localized regardless of its location in the network.

Then, localization of three leaks using the MFP 1D search is tested. Fig. 13 shows the results where the locations of three leaks are: (a) $x_1^{L1} = 1300$ m in Pipe 1, $x_2^{L2} = 800$ m in Pipe 2 and $x_4^{L3} = 200$ m in Pipe 4; (b) $x_2^{L1} = 700$ m in Pipe 2, $x_2^{L2} = 800$ m in Pipe 2 and $x_5^{L3} = 300$ m in Pipe 5; (c) $x_1^{L1} = 1300$ m in Pipe 1, $x_2^{L2} = 790$ m in Pipe 2 and $x_3^{L3} = 810$ m in Pipe 3. Fig. 13(a) demonstrates that, in the first case, the three leaks can be found from the three highest peaks of the MFP objective function. In the latter two cases, as shown in Fig. 13(b) and (c), one local maximum can be found near each leak, although other side-lobes prevent the accurate detection of the three leaks. Again, as demonstrated in Section 4.1.3, in order to accurately estimate the locations and sizes of all the leaks, the more elaborated model and inverse techniques as in [24,50,51] have to be used.

5. Experimental results

In this section, the MFP leakage localization method is tested in a pipe network built in the Water Resources Research Laboratory at the Hong Kong University of Science and Technology. The setup and sketch map of the pipe system can be seen in Fig. 14. The pipe lengths of the three pipes are $l_1 = 13.88$ m, $l_2 = 128$ m and $l_3 = 25$ m. The internal diameter of pipe is $d_1 = d_2 = d_3 = 0.0792$ m. The pipe material is high-density polyethylene (HDPE) and the viscoelastic coefficients in the generalized Kelvin-Voigt model are calibrated [25,32] and are shown in Table 1. The pipeline system is driven by a vertical multistage centrifugal pump connected to the upstream of Pipe 1. A valve is set at x_2^D to generate transient waves where the

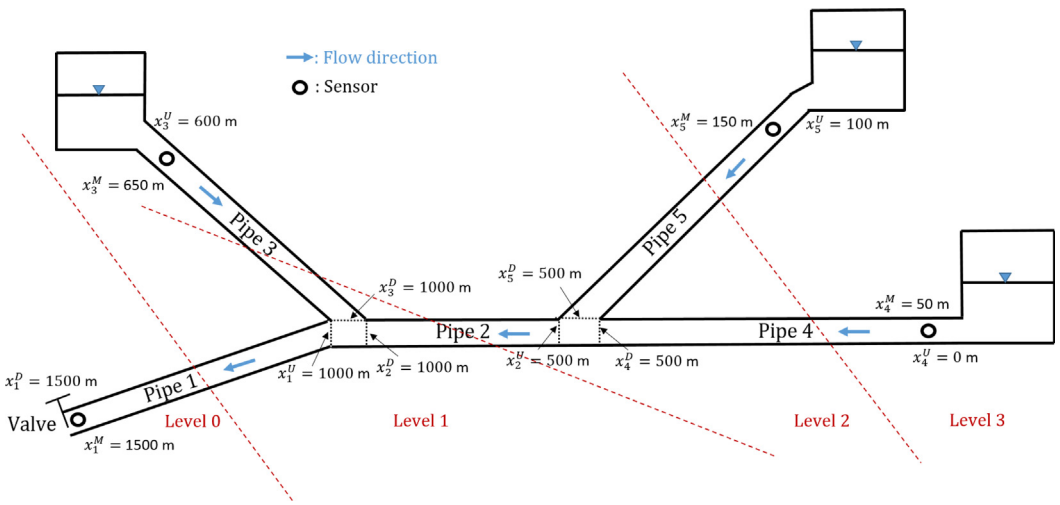

Fig. 11. Setup of the pipe network with five pipes in Section 4.2.

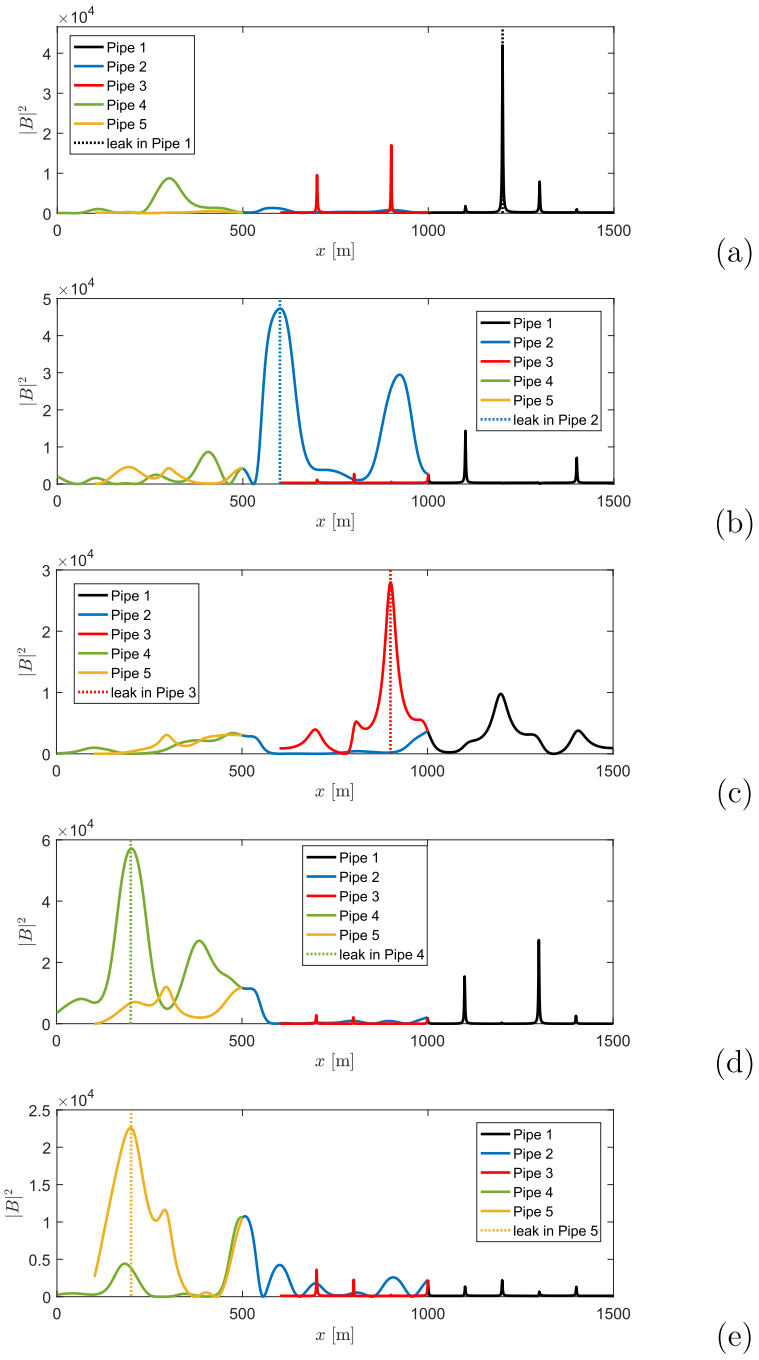

Fig. 12. Localization of one leak in the five-pipe network using MFP. The actual leak location is represented by the vertical dotted line.

closure time is approximately 0.06 s. Three pressure transducers (UNIK 5000, the maximum error is 0.04% of the full scale) are used to measure dynamic pressures at $x_1^M = 2.6$ m in Pipe 1, $x_2^M = 139.4$ m in Pipe 2 and $x_3^M = 17.9$ m in Pipe 3. A leak is located at $x_2^L = 43.9$ m in Pipe 2. The steady-state discharges from the leak and at the upstream of the leak are approximately 0.5×10^{-3} m^3/s and 1.5×10^{-3} m^3/s, respectively.

The boundary x_3^U of Pipe 3 is closed and the boundary condition $q(x_3^U) = 0$ is applied. Fig. 15 shows the measured time signal and the FRF of transient wave. In the leak localization using MFP, the FRF is cut from 7 Hz, i.e., $f \leq 7$ Hz is used, because after this frequency the signal is very noisy. Fig. 16 shows the leak localization result using MFP. The MFP objective function $|B|^2$ reaches maximum at 38.08 m in Pipe 2, i.e., the leak localization error is 5.8 m. To test the robustness of MFP, the tran-

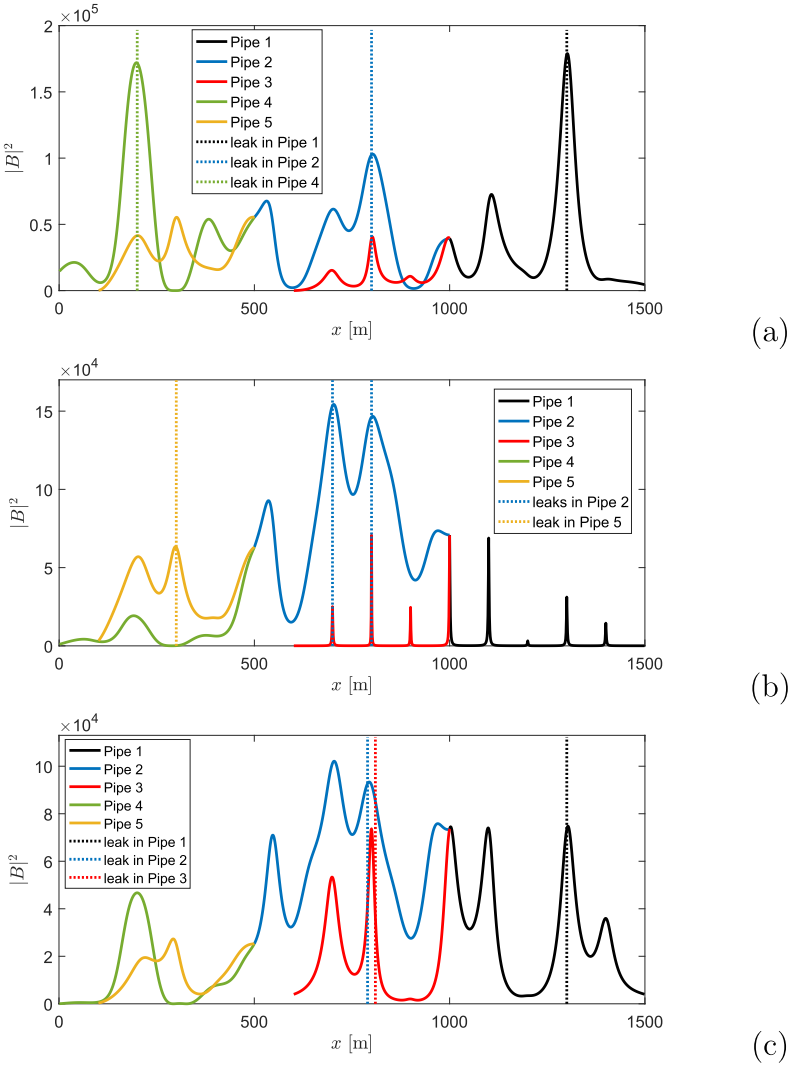

Fig. 13. Localization of three leaks in the five-pipe network using MFP. The actual leak locations are represented by the vertical dotted lines.

sient test is repeated a total of seven times. The shape of the MFP objective function of the other six tests is only slightly different from Fig. 16. The localization error in that six tests is respectively 5.6 m, 6.0 m, 6.4 m, 5.8 m, 6.2 m, 5.8 m. The leak localization of 5.5–6.5 m may stem from system bias or low resolution of the transient wave, which, according to the Nyquist-Shannon sampling theorem, is $\lambda_{\min}/2 = a/(2f_{\max}) \approx 365\text{m} \cdot \text{s}^{-1}/(2 \times 7\text{Hz}) = 26\text{m}$. Here, $a = 365\text{m/s}$ is the (elastic) wave speed estimated from the arrival time of transient wave at different sensors. Note that the leak localization error is much lower than $\lambda_{\min}/2$ meaning the error is acceptable in the sense of resolution of probing wave.

WTA and RFPP are also tested for leak localization using the same experimental data. Here, WTA only searches the leak in Pipe 2 (the section of signal in the enlarged plot in Fig. 15(a)); the latter signal corresponding to possible reflections in Pipe 1 and Pipe 3 are largely overlapped with the reflections from the interior junction and from the boundaries x_1^U and x_3^U, because in this system l_1 and l_3 are comparable with $\lambda_{\min}/2$. In this case, the leak localization error of WTA using the seven experimental results is 6.9 m, 6.7 m, 5.8 m, 8.0 m, 6.2 m, 5.8 m, 6.0 m, respectively. On the other hand, RFPP, which uses the first eight resonant frequency peaks, returns the leak localization result always at x_2^M, i.e., the error is 84 m. This is because the RFPP method in [31] does not model pipe wall viscoelasticity which induces a large modeling error.

6. Conclusion

This paper studies the leakage localization problem in tree-structured pipe networks using transient waves. A frequency-domain wave propagation model in a general tree-structured pipe network is derived, where the leak parameters (location

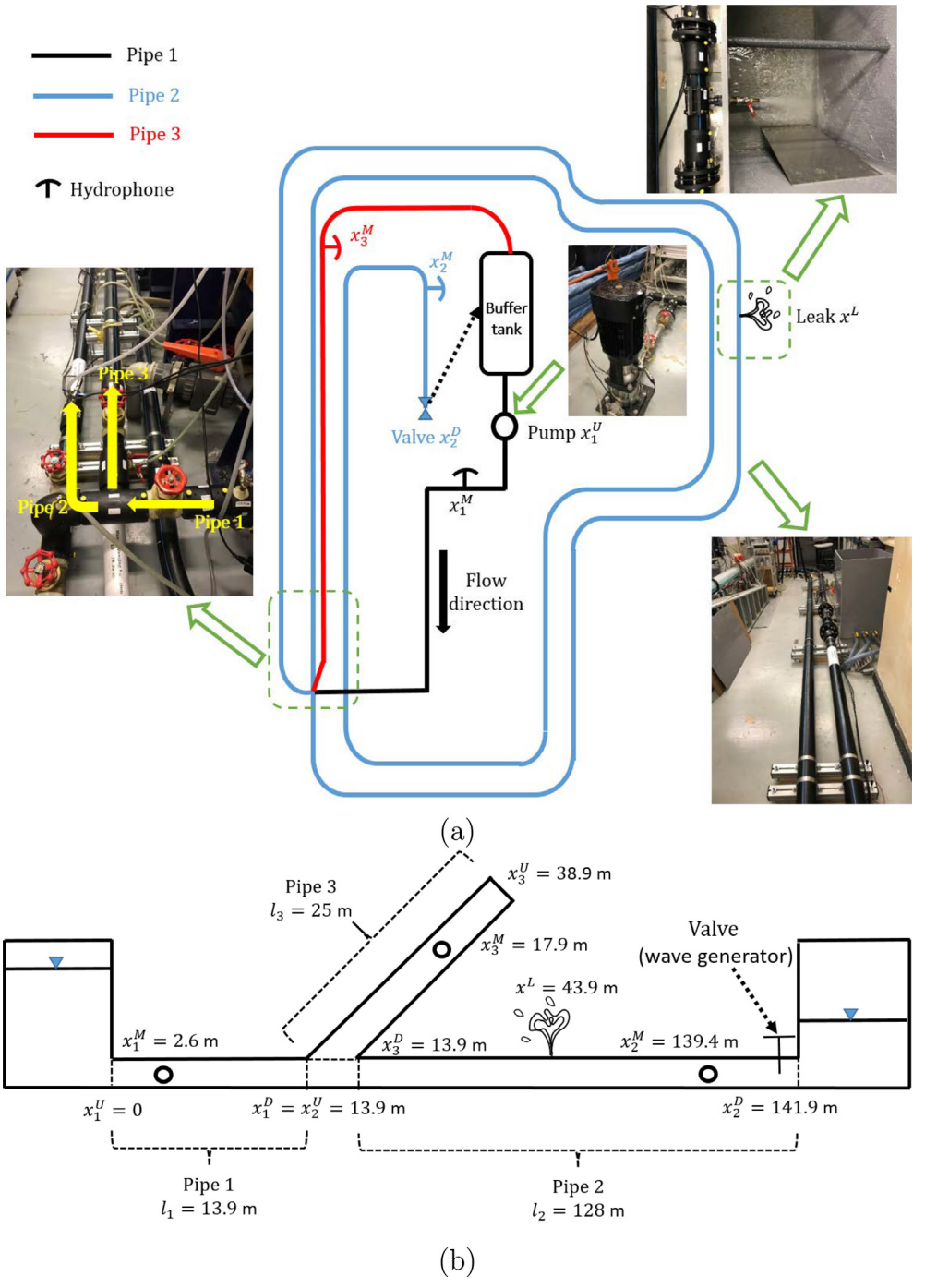

Fig. 14. Setup of the pipe system in the Water Resources Research Laboratory at Hong Kong University of Science and Technology.

Table 1
Coefficients for pipe wall viscoelasticity in the experiments at the Hong Kong University of Science and Technology.

$\nu = 0.43$	$\kappa = 2.1 \times 10^9$ Pa	$\rho = 10^3$ kg/m^3
$D = 79.2$ mm	$e = 5.4$ mm	$J_0 = 5.8 \times 10^{-10}$ Pa^{-1}
$J_1 = 1.96 \times 10^{-10}$ Pa^{-1}	$\tau_1 = 0.038$ s	$J_2 = 1.10 \times 10^{-10}$ Pa^{-1}
$\tau_2 = 0.6$ s	$J_3 = 9.05 \times 10^{-12}$ Pa^{-1}	$\tau_3 = 1.5$ s

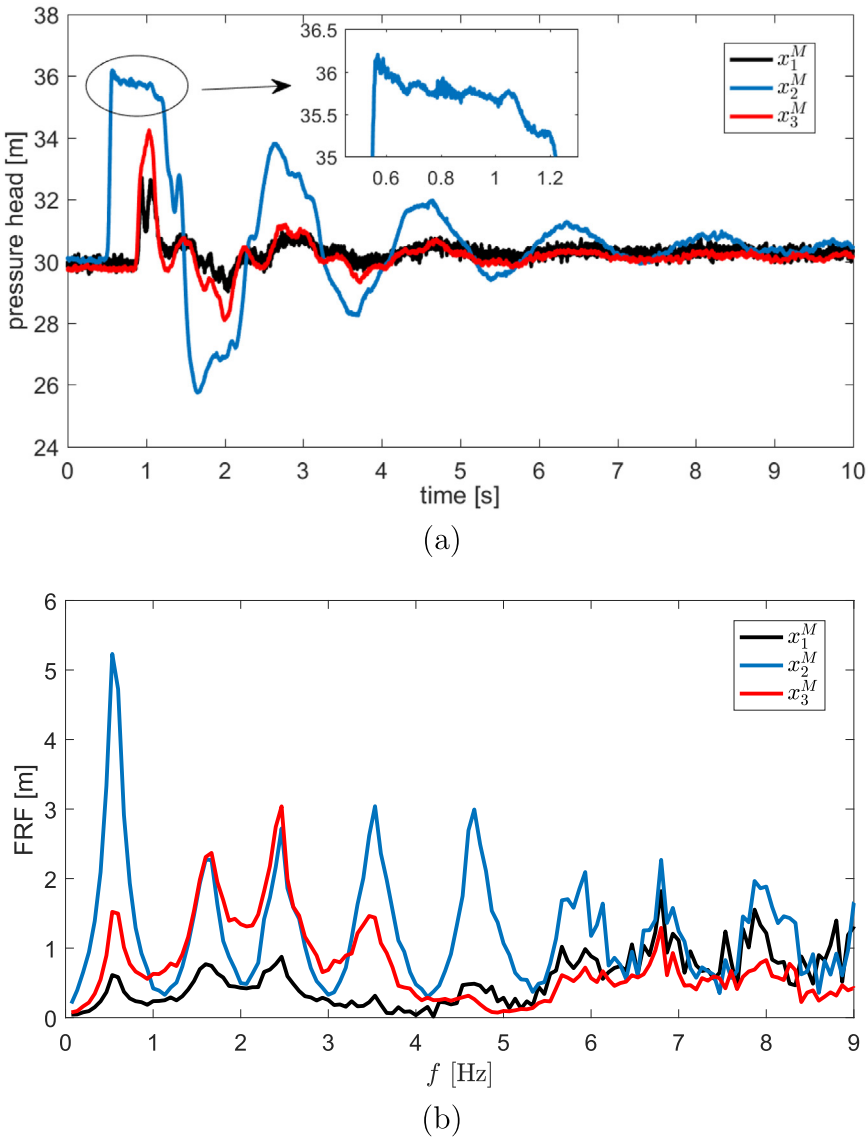

Fig. 15. Experimental measurements obtained from the sensor x_1^M, x_2^M, x_3^M in the time domain (a) and in the frequency domain (b).

and size) are factorized. By virtue of this factorized model, an efficient leak localization method in a pipe network is realized based on the matched-field processing (MFP) principle.

The efficiency of the MFP leak localization method is illustrated via numerical simulation and laboratory experiments. Numerical examples show that the MFP method uniquely identifies a single leak anywhere in a network and it is more robust in noisy environments than the existing techniques. Two or three leaks can also be localized by the proposed method, if their distance is greater than half minimum wavelength of probing transient wave. Experimental data obtained from a viscoelastic pipe network demonstrate that the proposed method can successfully find the leak even with measured signal contaminated by noise.

Generalization of the proposed methodology to more general pipe networks with loop structures would be an interesting and logical next step. In loop-structured networks, the path uniqueness from each boundary to any location in the system is no longer valid, therefore the factorized form of the model cannot be straightforwardly obtained. This problem is currently under investigation by the authors. Moreover, in the present paper, only purely random noise is considered in the MFP method. In real urban water supply pipe networks where the scale is normally much larger and the structure is more complex than the examples in this paper, the uncertainties due to water demand from the consumer-side, imprecise knowledge of system attribute, and unknown boundary characterization may play a more crucial role. Study of these effects of uncer-

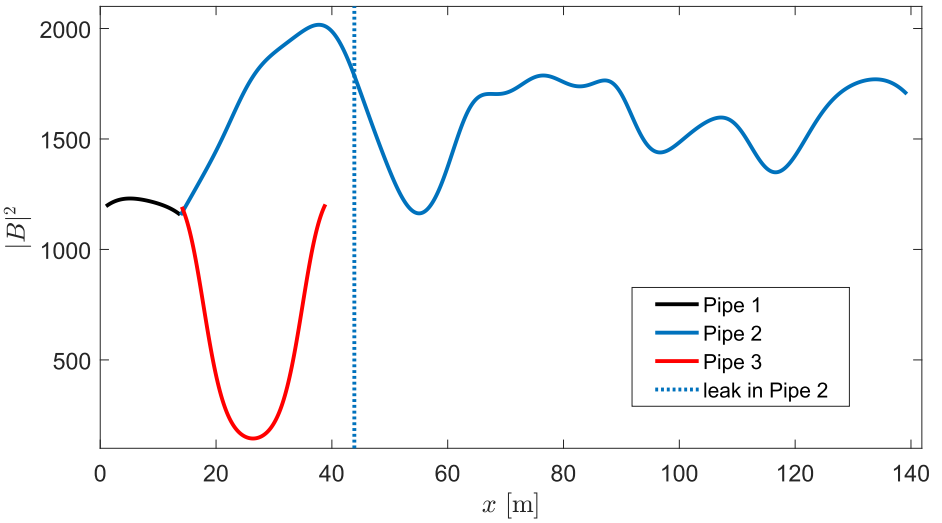

Fig. 16. Leak localization using MFP with experimental data.

tainty in real water-pipe networks and quantifying them in the leak localization procedure would also be an important future work.

CRediT authorship contribution statement

Xun Wang: Conceptualization, Methodology, Software, Data curation, Writing - original draft, Writing - review & editing. **G. Adriana Camino:** Data curation, Writing - review & editing. **Tong-Chuan Che:** Software, Writing - review & editing. **Mohamed S. Ghidaoui:** Methodology, Writing - review & editing.

Declaration of Competing Interest

The authors declare that they have no known competing financial interests or personal relationships that could have appeared to influence the work reported in this paper.

Acknowledgement

This work has been supported by research grants from the Research Grant Council of the Hong Kong SAR, China (Project No. T21-602/15R). The authors would like to thank Prof. T. C. Yang (Zhejiang University) for discussion.

Appendix A. Wave speed in elastic and viscoelastic pipes

In the i-th pipe, if the pipe material is elastic, the wave speed is constant:

$$a_i = \left(\rho\left(\frac{1}{\kappa} + (1-\nu^2)\frac{d_i}{e_i}J_0\right)\right)^{-\frac{1}{2}}, \tag{A.1}$$

where κ and ρ are the bulk modulus and density of water, ν is the Poisson's ratio of pipe material, e_i is the pipe wall thickness, and $J_0 = 1/E$ is the instantaneous creep-compliance where E is the Young's modulus of pipe wall elasticity. In the case of viscoelastic pipe, the pipe wall deformation during transient wave propagation is modeled by the generalized Kelvin-Voigt model [52–59]. It is shown in [25] that the viscoelastic behavior can be equivalently quantified by changing the wave speed to be frequency-dependent:

$$a_i(\omega) = \left(\rho\left(\frac{1}{\kappa} + (1-\nu^2)\frac{d_i}{e_i}\left(J_0 + \sum_{j=1}^{N_{kv}}\frac{J_j}{1+\mathrm{i}\omega\tau_j}\right)\right)\right)^{-\frac{1}{2}}, \tag{A.2}$$

where, N_{kv} is the truncated order, J_j and τ_j are coefficients of the generalized Kelvin-Voigt model.

Appendix B. Explicit form of Eq. (16) in Example 3

Expanding Eqs. (17), (19), (21), and (23), we obtain

$$\begin{aligned} h^{NL}(x^M) = &-Z_2 \sinh\left(\mu_2(x^M - x_2^U)\right)\cosh\left(\mu_1(x_1^D - x_1^U)\right)q(x_1^U) - Z_1 \cosh\left(\mu_2(x^M - x_2^U)\right)\sinh\left(\mu_1(x_1^D - x_1^U)\right)q(x_1^U) \\ &+ \frac{Z_2}{Z_1}\sinh\left(\mu_2(x^M - x_2^U)\right)\sinh\left(\mu_1(x_1^D - x_1^U)\right)h(x_1^U) + \cosh\left(\mu_2(x^M - x_2^U)\right)\cosh\left(\mu_1(x_1^D - x_1^U)\right)h(x_1^U) \\ &+ Z_2 \sinh\left(\mu_2(x^M - x_2^U)\right)\cosh\left(\mu_3(x_3^D - x_3^U)\right)q(x_3^U) - \frac{Z_2}{Z_3}\sinh\left(\mu_2(x^M - x_2^U)\right)\sinh\left(\mu_3(x_3^D - x_3^U)\right)h(x_3^U) \end{aligned} \tag{B.1}$$

and

$$G(x^L; x^M) = \begin{cases} \sqrt{\frac{g}{2(H_0^L - z^L)}}G_1(x^L; x^M), & \text{if } x^L \text{ in Pipe 1} \\ \sqrt{\frac{g}{2(H_0^L - z^L)}}G_2(x^L; x^M), & \text{if } x^L \text{ in Pipe 2} \\ \sqrt{\frac{g}{2(H_0^L - z^L)}}G_3(x^L; x^M), & \text{if } x^L \text{ in Pipe 3} \end{cases}, \tag{B.2}$$

where

$$\begin{aligned} G_1(x^L; x^M) = &-Z_1 Z_2 \sinh\left(\mu_2(x^M - x_2^U)\right)\sinh\left(\mu_1(x^L - x_1^U)\right)\cosh\left(\mu_1(x_1^D - x^L)\right)q(x_1^U) \\ &- Z_1^2 \cosh\left(\mu_2(x^M - x_2^U)\right)\sinh\left(\mu_1(x^L - x_1^U)\right)\sinh\left(\mu_1(x_1^D - x^L)\right)q(x_1^U) \\ &- Z_2 \sinh\left(\mu_2(x^M - x_2^U)\right)\cosh\left(\mu_1(x^L - x_1^U)\right)\cosh\left(\mu_1(x_1^D - x^L)\right)h(x_1^U) \\ &+ Z_1 \cosh\left(\mu_2(x^M - x_2^U)\right)\cosh\left(\mu_1(x^L - x_1^U)\right)\sinh\left(\mu_1(x_1^D - x^L)\right)h(x_1^U), \end{aligned} \tag{B.3}$$

$$\begin{aligned} G_2(x^L; x^M) = &-Z_2^2 \sinh\left(\mu_2(x^L - x_2^U)\right)\sinh\left(\mu_2(x^M - x_2^L)\right)\cosh\left(\mu_1(x_1^D - x_1^U)\right)q(x_1^U) \\ &- Z_1 Z_2 \cosh\left(\mu_2(x^L - x_2^U)\right)\sinh\left(\mu_2(x^M - x_2^L)\right)\sinh\left(\mu_1(x_1^D - x_1^U)\right)q(x_1^U) \\ &+ \frac{Z_2^2}{Z_1}\sinh\left(\mu_2(x^L - x_2^U)\right)\sinh\left(\mu_2(x^M - x_2^L)\right)\sinh\left(\mu_1(x_1^D - x_1^U)\right)h(x_1^U) \\ &+ Z_2 \cosh\left(\mu_2(x^L - x_2^U)\right)\sinh\left(\mu_2(x^M - x_2^L)\right)\cosh\left(\mu_1(x_1^D - x_1^U)\right)h(x_1^U) \\ &+ Z_2^2 \sinh\left(\mu_2(x^L - x_2^U)\right)\sinh\left(\mu_2(x^M - x_2^L)\right)\cosh\left(\mu_3(x_3^D - x_3^U)\right)q(x_3^U) \\ &- \frac{Z_2^2}{Z_3}\sinh\left(\mu_2(x^L - x_2^U)\right)\sinh\left(\mu_2(x^M - x_2^L)\right)\sinh\left(\mu_3(x_3^D - x_3^U)\right)h(x_3^U), \end{aligned} \tag{B.4}$$

and

$$\begin{aligned} G_3(x^L; x^M) = &-Z_2 Z_3 \sinh\left(\mu_2(x^M - x_2^U)\right)\sinh\left(\mu_3(x^L - x_3^U)\right)\cosh\left(\mu_3(x_3^D - x^L)\right)q(x_3^U) \\ &+ Z_2 \sinh\left(\mu_2(x^M - x_2^U)\right)\cosh\left(\mu_3(x^L - x_3^U)\right)\cosh\left(\mu_3(x_3^D - x^L)\right)h(x_3^U). \end{aligned} \tag{B.5}$$

Appendix C. Matched-field processing for estimating leak location and size

A unit vector $\mathbf{w} = (w_1, \ldots, w_K)^\top$ ($|\mathbf{w}| = 1$) is adjusted to have the same direction as the measurement $\Delta\mathbf{h}$ in the K-dimensional complex vector space. The inner product of the weighting vector $\mathbf{w}$ and $\Delta\mathbf{h}$ is

$$B \equiv < \mathbf{w}, \Delta\mathbf{h} > = \mathbf{w}^H \Delta\mathbf{h} \in \mathbb{C}. \tag{C.1}$$

The optimal weight is obtained by solving for $\mathbf{w}$ which maximizes

$$|B|^2 = |\mathbf{w}^H \Delta\mathbf{h}|^2 = \mathbf{w}^H \Delta\mathbf{h}\Delta\mathbf{h}^H \mathbf{w}. \tag{C.2}$$

Inserting the model of $\Delta\mathbf{h}$, i.e., Eq. (38), into Eq. (C.2) and maximizing its expectation with $\mathbf{w}$, the optimal weight is obtained:

$$\hat{\mathbf{w}} = \arg\max_{\mathbf{w}} \mathbb{E}\left(|B|^2\right) = \arg\max_{\mathbf{w}}\left(\left(s^L\right)^2 \mathbf{w}^H \mathbf{G}\mathbf{G}^H \mathbf{w} + \sigma^2\right) = \arg\max_{\mathbf{w}}\left(\mathbf{w}^H \mathbf{G}\mathbf{G}^H \mathbf{w}\right) = \pm\frac{\mathbf{G}}{\sqrt{\mathbf{G}^H\mathbf{G}}}. \tag{C.3}$$

Note that the optimal $\mathbf{w}$ is a vector having the same direction as $\mathbf{G}$. Then, the leakage location can be estimated by substituting Eq. (C.3) back to Eq. (C.2):

$$\widehat{x^L} = \arg\max_{x^L} \frac{\Delta\mathbf{h}^H \mathbf{G}(x^L)\mathbf{G}^H(x^L)\Delta\mathbf{h}}{\mathbf{G}^H(x^L)\mathbf{G}(x^L)}. \tag{C.4}$$

It can be shown that Eq. (C.4) is also a maximum likelihood estimate of the leak position [60,61,6]. Furthermore, the leak size can be estimated via the maximum likelihood principle:

$$\widehat{s^L} = \frac{\mathbf{G}^H\left(\widehat{x^L}\right)\Delta\mathbf{h}}{\mathbf{G}^H\left(\widehat{x^L}\right)\mathbf{G}\left(\widehat{x^L}\right)}. \tag{C.5}$$

References

[1] A.F. Colombo, P. Lee, B.W. Karney, A selective literature review of transient-based leak detection methods, J. Hydro-Environ. Res. 2 (4) (2009) 212–227.
[2] J.A. Liggett, L.-C. Chen, Inverse transient analysis in pipe networks, J. Hydraul. Eng. 120 (8) (1994) 934–955.
[3] J.P. Vítkovský, A.R. Simpson, M.F. Lambert, Leak detection and calibration using transients and genetic algorithms, J. Water Resour. Planning Manage. 126 (4) (2000) 262–265.
[4] P.J. Lee, J.P. Vítkovský, M.F. Lambert, A.R. Simpson, J.A. Liggett, Leak location using the pattern of the frequency response diagram in pipelines: a numerical study, J. Sound Vib. 284 (3) (2005) 1051–1073.
[5] M. Ferrante, B. Brunone, S. Meniconi, Wavelets for the analysis of transient pressure signals for leak detection, J. Hydraul. Eng. 133 (11) (2007) 1274–1282.
[6] X. Wang, M.S. Ghidaoui, Pipeline leak detection using the matched-field processing method, J. Hydraul. Eng. 144 (6) (2018) 04018030.
[7] J.C.P. Liou, Pipeline leak detection by impulse response extraction, J. Fluids Eng. 120 (4) (1998) 833–838.
[8] B. Brunone, Transient test-based technique for leak detection in outfall pipes, J. Water Resour. Planning Manage. 125 (5) (1999) 302–306.
[9] B. Brunone, M. Ferrante, Detecting leaks in pressurised pipes by means of transients, J. Hydraul. Res. 39 (5) (2001) 539–547.
[10] S. Meniconi, B. Brunone, M. Ferrante, C. Capponi, C.A. Carrettini, C. Chiesa, D. Segalini, E.A. Lanfranchi, Anomaly pre-localization in distribution–transmission mains by pump trip: preliminary field tests in the milan pipe system, J. Hydroinf. 17 (3) (2015) 377–389.
[11] S.T.N. Nguyen, J. Gong, M.F. Lambert, A.C. Zecchin, A.R. Simpson, Least squares deconvolution for leak detection with a pseudo random binary sequence excitation, Mech. Syst. Signal Process. 99 (2018) 846–858.
[12] W. Mpesha, S.L. Gassman, M.H. Chaudhry, Leak detection in pipes by frequency response method, J. Hydraul. Eng. 127 (2) (2001) 134–147.
[13] M. Ferrante, B. Brunone, Pipe system diagnosis and leak detection by unsteady-state tests. 1. harmonic analysis, Adv. Water Resour. 26 (1) (2003) 95–105.
[14] D. Covas, H. Ramos, A.B. De Almeida, Standing wave difference method for leak detection in pipeline systems, J. Hydraul. Eng. 131 (12) (2005) 1106–1116.
[15] P.J. Lee, J.P. Vítkovský, M.F. Lambert, A.R. Simpson, J.A. Liggett, Frequency domain analysis for detecting pipeline leaks, J. Hydraul. Eng. 131 (7) (2005) 596–604.
[16] P.J. Lee, M.F. Lambert, A.R. Simpson, J.P. Vítkovský, J. Liggett, Experimental verification of the frequency response method for pipeline leak detection, J. Hydraul. Res. 44 (5) (2006) 693–707.
[17] A.M. Sattar, M.H. Chaudhry, Leak detection in pipelines by frequency response method, J. Hydraul. Res. 46 (sup1) (2008) 138–151.
[18] H.-F. Duan, P.J. Lee, M.S. Ghidaoui, Y.-K. Tung, Leak detection in complex series pipelines by using the system frequency response method, J. Hydraul. Res. 49 (2) (2011) 213–221.
[19] G.A. Nash, B.W. Karney, Efficient inverse transient analysis in series pipe systems, J. Hydraul. Eng. 125 (7) (1999) 761–764.
[20] D. Covas, H. Ramos, N. Graham, C. Maksimovic, Application of hydraulic transients for leak detection in water supply systems, Water Sci. Technol.: Water Supply 4 (5–6) (2005) 365–374.
[21] D. Covas, H. Ramos, Case studies of leak detection and location in water pipe systems by inverse transient analysis, J. Water Resour. Planning Manage. 136 (2) (2010) 248–257.
[22] A.K. Soares, D.I.C. Covas, L.F.R. Reis, Leak detection by inverse transient analysis in an experimental PVC pipe system, J. Hydroinf. 13 (2) (2011) 153–166.
[23] I. Rubio Scola, G. Besançon, D. Georges, Blockage and leak detection and location in pipelines using frequency response optimization, J. Hydraul. Eng. 143 (1) (2016) 04016074.
[24] X. Wang, M.S. Ghidaoui, Identification of multiple leaks in pipeline: Linearized model, maximum likelihood, and super-resolution localization, Mech. Syst. Signal Process. 107 (2018) 529–548.
[25] X. Wang, J. Lin, A. Keramat, M.S. Ghidaoui, S. Meniconi, B. Brunone, Matched-field processing for leak localization in a viscoelastic pipe: An experimental study, Mech. Syst. Signal Process. 124 (2019) 459–478.
[26] X. Wang, D.P. Palomar, L. Zhao, M.S. Ghidaoui, R.D. Murch, Spectral-based methods for pipeline leakage localization, J. Hydraul. Eng. 145 (3) (2019) 04018089.
[27] B. Zhou, A. Liu, X. Wang, Y. She, V. Lau, Compressive sensing-based multiple-leak identification for smart water supply systems, IEEE Internet Things J. 5 (2) (2018) 1228–1241.
[28] M. Ferrante, B. Brunone, S. Meniconi, Leak detection in branched pipe systems coupling wavelet analysis and a lagrangian model, J. Water Supply: Res. Technol.-AQUA 58 (2) (2009) 95–106.
[29] S.B. Beck, M.D. Curren, N.D. Sims, R. Stanway, Pipeline network features and leak detection by cross-correlation analysis of reflected waves, J. Hydraul. Eng. 131 (8) (2005) 715–723.
[30] M.F. Ghazali, S.B.M. Beck, J.D. Shucksmith, J.B. Boxall, W.J. Staszewski, Comparative study of instantaneous frequency based methods for leak detection in pipeline networks, Mech. Syst.Signal Process. 29 (2012) 187–200.
[31] H.-F. Duan, Transient frequency response based leak detection in water supply pipeline systems with branched and looped junctions, J. Hydroinf. 19 (1) (2017) 17–30.
[32] X. Wang, J. Lin, M.S. Ghidaoui, S. Meniconi, B. Brunone, Estimating viscoelasticity of pipes with unknown leaks, Mech. Syst. Signal Process. 143 (2020) 106821.
[33] Z.S. Kapelan, D.A. Savic, G.A. Walters, A hybrid inverse transient model for leakage detection and roughness calibration in pipe networks, J. Hydraul. Res. 41 (5) (2003) 481–492.
[34] C. Capponi, M. Ferrante, A.C. Zecchin, J. Gong, Leak detection in a branched system by inverse transient analysis with the admittance matrix method, Water Resour. Manage. 31 (13) (2017) 4075–4089.
[35] S. Kim, Impedance method for abnormality detection of a branched pipeline system, Water Resour. Manage. 30 (3) (2016) 1101–1115.
[36] A.C. Zecchin, M.F. Lambert, A.R. Simpson, L.B. White, Frequency-domain modeling of transients in pipe networks with compound nodes using a laplace-domain admittance matrix, J. Hydraul. Eng. 136 (10) (2010) 739–755.
[37] A.C. Zecchin, L.B. White, M.F. Lambert, A.R. Simpson, Parameter identification of fluid line networks by frequency-domain maximum likelihood estimation, Mech. Syst. Signal Process. 37 (1) (2013) 370–387.
[38] M.H. Chaudhry, Applied Hydraulic Transients, third ed., Springer, 2014.
[39] E.B. Wylie and V.L. Streeter. Fluid transients. New York, McGraw-Hill International Book Co., 1, 1978..
[40] E. Blasten, F. Zouari, M. Louati, and M.S. Ghidaoui. Blockage detection in networks: The area reconstruction method. arXiv preprint arXiv:1909.05497, 2019..

[41] M.I. Belishev, N. Wada, On revealing graph cycles via boundary measurements, Inverse Prob. 25 (10) (2009) 105011.
[42] P.J. Lee. Using system response functions of liquid pipelines for leak and blockage detection (Ph.D. thesis). The University of Adelaide, Adelaide AU, 2005..
[43] X. Wang, M.S. Ghidaoui, P.J. Lee, Linear model and regularization for transient wave–based pipeline-condition assessment, J. Water Resour. Planning Manage. 146 (5) (2020) 04020028.
[44] X. Wang, J. Lin, M.S. Ghidaoui, Usage and effect of multiple transient tests for pipeline leak detection, J. Water Resour. Planning Manage. (2020), https://doi.org/10.1061/(ASCE)WR.1943-5452.0001284, in press.
[45] M.H. Ranginkaman, A. Haghighi, P.J. Lee, Frequency domain modelling of pipe transient flow with the virtual valves method to reduce linearization errors, Mech. Syst. Signal Process. 131 (2019) 486–504.
[46] A. Kashima, P.J. Lee, R. Nokes, Numerical errors in discharge measurements using the KDP method, J. Hydraul. Res. 50 (1) (2012) 98–104.
[47] A. Kashima, P.J. Lee, M.S. Ghidaoui, M. Davidson, Experimental verification of the kinetic differential pressure method for flow measurements, J. Hydraul. Res. 51 (6) (2013) 634–644.
[48] A. Kessy, A. Lewin, K. Strimmer, Optimal whitening and decorrelation, Am. Statistician 72 (4) (2018) 309–314.
[49] X. Wang, M. Waqar, H.-C. Yan, M. Louati, M.S. Ghidaoui, P.J. Lee, S. Meniconi, B. Brunone, B. Karney, Pipeline leak localization using matched-field processing incorporating prior information of modeling error, Mech. Syst. Signal Process. 143 (2020) 106849.
[50] X. Wang, M.S. Ghidaoui, Identification of multiple leaks in pipeline II: Iterative beamforming and leak number estimation, Mech. Syst. Signal Process. 119 (2019) 346–362.
[51] X. Wang, M.S. Ghidaoui, J. Lin, Identification of multiple leaks in pipeline III: Experimental results, Mech. Syst. Signal Process. 130 (2019) 395–408.
[52] G. Pezzinga, P. Scandura, Unsteady flow in installations with polymeric additional pipe, J. Hydraul. Eng. 121 (11) (1995) 802–811.
[53] D. Covas, I. Stoianov, H. Ramos, N. Graham, C. Maksimovic, The dynamic effect of pipe-wall viscoelasticity in hydraulic transients. Part I–experimental analysis and creep characterization, J. Hydraul. Res. 42 (5) (2004) 517–532.
[54] D. Covas, I. Stoianov, J.F. Mano, H. Ramos, N. Graham, C. Maksimovic, The dynamic effect of pipe-wall viscoelasticity in hydraulic transients. Part II–model development, calibration and verification, J. Hydraul. Res. 43 (1) (2005) 56–70.
[55] A. Keramat, A.S. Tijsseling, Q. Hou, A. Ahmadi, Fluid–structure interaction with pipe-wall viscoelasticity during water hammer, J. Fluids Struct. 28 (2012) 434–455.
[56] H.-F. Duan, M. Ghidaoui, P.J. Lee, Y.-K. Tung, Unsteady friction and visco-elasticity in pipe fluid transients, J. Hydraul. Res. 48 (3) (2010) 354–362.
[57] S. Meniconi, B. Brunone, M. Ferrante, C. Massari, Numerical and experimental investigation of leaks in viscoelastic pressurized pipe flow, Drinking Water Eng. Sci. 6 (1) (2013) 11–16.
[58] S. Evangelista, A. Leopardi, R. Pignatelli, G. de Marinis, Hydraulic transients in viscoelastic branched pipelines, J. Hydraul. Eng. 141 (8) (2015) 04015016.
[59] G. Pezzinga, B. Brunone, S. Meniconi, Relevance of pipe period on kelvin-voigt viscoelastic parameters: 1D and 2D inverse transient analysis, J. Hydraul. Eng. 142 (12) (2016) 04016063.
[60] H. Krim, M. Viberg, Two decades of array signal processing research, IEEE Signal Process. Mag. 13 (4) (1996) 67–94.
[61] X. Wang, B. Quost, J.-D. Chazot, J. Antoni, Estimation of multiple sound sources with data and model uncertainties using the EM and evidential EM algorithms, Mech. Syst. Signal Process. 66–67 (2016) 159–177.